

# Weak Gravitational Lensing of Schwarzschild and Charged Black Holes Embedded in Perfect Fluid Dark Matter Halo

Chen-Kai Qiao\* and Mi Zhou†

*College of Science, Chongqing University of Technology, Banan, Chongqing, 400054, China*

(Dated: December 29, 2022)

The dark matter and dark energy dominate the behavior of our universe. The unknown dark matter usually forms halos in large number of galaxies. Properties of dark matter halo can be revealed and understood from the gravitational lensing observations. In this work, a comprehensive study on the weak gravitational lensing of black hole embedded in dark matter halos is presented. To effectively model the supermassive black hole in galaxy center (which is surrounded by dark matter halo) in a simple way, we use the Schwarzschild black hole and charged Reissner-Nordström black hole embedded in a perfect fluid dark matter halo. In the present work, several key quantities in weak gravitational lensing (gravitational deflection angle of light, photon sphere, black hole shadow radius, gravitational lens equation and Einstein ring) are calculated and analyzed analytically and numerically. The results in our work indicate that the dark matter can greatly influence the gravitational lensing of central black holes.

Keywords: Black Hole, Weak Gravitational Lensing; Gauss-Bonnet Theorem; Dark Matter Halo

## I. INTRODUCTION

Black hole is a significantly important subject in the gravity theory. Significantly important information on gravitation, thermodynamics and quantum effects in curved spacetime can be revealed through black holes [1–4]. A number of progresses on theoretical and observational explorations of black holes have been witnessed in the past several years. The gravitational wave signals were detected by LIGO and Virgo from the merging of binary black holes [5]. The high resolution black hole images at the center of M87 and our galaxy were successfully observed by Event Horizon Telescope [6, 7].

Dark matter is one of the most attractive topics among elementary particle physics, astrophysics, astronomy and cosmology. The accumulating evidences for existence of dark matter have been found from the rotation curves of spiral galaxies [8, 9], gravitational lensing [10], large scale structure formation of the universe [11], cosmic microwave background and baryon acoustic oscillations [12, 13]. The combined observations from cosmic microwave background indicates that 26.8% of our universe is made up of dark matter, and 68.3% of our universe is made up of dark energy [13]. The dark matter could affect the evolution of our universe, therefore it is a crucial factor which determines the fate of our universe. The most favorable candidates for dark matter are the some unknown particles predicted by theories beyond the standard model, such as weakly interacting massive particles, axions, sterile neutrinos, dark photons, millicharged particles [14–20]. These unknown dark matters usually form dark matter halos in large number of galaxies [21–23]. In this way, the supermassive black holes in the center of

galaxies are surrounded by these dark matter halos. In this way, studying and analyzing the effects of dark matter halo on supermassive black holes in galaxy center is of great significance. Recently, a number of works emerged to study the dark matter effects on black holes, such as the circular geodesics [24, 25], black hole shadow [26–32], gravitational lensing [33–38], accretion disk [39], thermodynamics [40, 41], quasi-normal mode [42, 43], black hole echoes [44] and black hole merging process [45].

The properties of unknown dark matter (as well as its halo in galaxies) could be investigated in a number of observations. The gravitational lensing is one of the most important method. In the past few decades, the weak gravitational lensing is becoming an important tool in astronomy and cosmology to test gravity theories and astrophysical models [46–49]. Particularly, recent studies suggest that the dark matter distribution in galaxies can be revealed from gravitational lensing observations [10, 49, 50]. The amounts and properties of dark matter halo in galaxies and galaxies clusters are strongly constrained by a number of weak and strong gravitational observations.

In this work, we aim to get a comprehensive study of the dark matter halo effects on gravitational bending and weak gravitational lensing for central supermassive black holes in dark matter halo. We choose two classical renowned black holes — Schwarzschild black hole and charged Reissner-Nordström (RN) black hole — to carry out the calculations. As the most popular and representative example in gravity theory and general relativity, the Schwarzschild black hole and charged RN black hole could reveal most of universal properties of more complex and realistic black holes. Further, we propose that the dark matter which surrounds central black hole is modeled by perfect fluid with energy-momentum tensor given by  $T_{\mu\nu} = (\rho + p)u_\mu u_\nu + pg_{\mu\nu}$ . This kind of dark matter is called as perfect fluid dark matter (PFDM) in literature [51]. Concretely, in the present work, the gravitational

\* [chenkaiqiao@cqut.edu.cn](mailto:chenkaiqiao@cqut.edu.cn)

† [lilyzm@cqut.edu.cn](mailto:lilyzm@cqut.edu.cn)

deflection angle of light, photon spheres, shadow radius, weak gravitational lensing equations and Einstein rings are calculated analytically and numerically. We focus ourselves on the dark matter effects on central black holes in gravitational bending and weak gravitational lensing. Hopefully, the conclusions generated from these classical black hole could give hints on gravitational lensing of more complex black holes embedded in dark matter halos.

In the present work, we adopt two approaches to calculate the gravitational deflection angle of light. One is a geometric approach developed by G. W. Gibbons and M. C. Werner [52], in which the gravitational deflection angle of light is calculated by applying Gauss-Bonnet theorem in differential geometry and topology. The other is the conventional approach in gravity theory, in which the gravitational deflection angle is calculated by solving the trajectories of particle orbits (which are null geodesics for photon orbits). In the analysis of photon spheres and black hole shadow radius, one should calculate the effective potential of test particle moving in the gravitational field and find its local maximum points. Besides, we can also use a geometric approach developed by Qiao *et al.* [53–55], which determine the stable and unstable photon sphere using Gaussian curvature and geodesic curvature. This approach could get completely equivalent results to the conventional approach (based on effective potential). Finally, in the calculation of Einstein ring angles, we numerically solve the gravitational lens equation in weak gravitational lensing cases.

This paper is organized in the following way. The section I gives the background introductions and motivations of this work. In section II, the Schwarzschild black hole and charged RN black hole embedded in perfect fluid dark matter (PFDM) halo is reviewed. In section III, we give the description of the theoretical framework. The approaches to calculate the gravitational deflection angle, photon sphere, black hole shadow radius, lens equation and Einstein ring angle are presented systematically in this section. In section IV, we present the results on gravitational deflection angle of light for Schwarzschild black hole and charged RN black hole embedded in PFDM. Section V gives the numerical results on photon spheres and black hole shadows. In section VI, we briefly discuss the observable in weak gravitational lensing, including lens equation and Einstein ring angle. The summary and conclusions are given in section VII. In this work, the natural unit  $G = c = 1$  is adopted.

## II. SCHWARZSCHILD AND CHARGED REISSNER-NORDSTRÖM (RN) BLACK HOLE EMBEDDED IN DARK MATTER HALO

In this section, we give an introduction of the spacetime metric for black holes embedded in dark matter halos. In the present work, we concentrate ourselves on two classical hole holes — Schwarzschild black hole and charged Reissner-Nordström (RN) black hole — embed-

ded in dark matter halo. As typical example in general relativity, the Schwarzschild black hole and charged RN black hole could reflect most of universal properties for more complex and realistic black holes. A comprehensive understanding of such black holes could provide useful information for other more complex supermassive black holes.

The spacetime generated by Schwarzschild black hole and charged RN black hole are spherically symmetric. Furthermore, the modern astrophysical observations show that dark matter halos in many galaxies are nearly spherically symmetric [21, 22]. Therefore, for simplicity, we can use the spherically symmetric spacetime to give a description of the supermassive black hole embedded in dark matter halos.

$$\begin{aligned} d\tau^2 &= g_{\mu\nu} dx^\mu dx^\nu \\ &= f(r) dt^2 - \frac{1}{f(r)} dr^2 - r^2(d\theta^2 + \sin^2\theta d\phi^2) \end{aligned} \quad (1)$$

the function  $f(r)$  is defined through the black hole mass  $M$ , black hole charge  $Q$  and contributions from dark matter halo:

$$f(r) = 1 - \frac{2M}{r} + \frac{Q^2}{r^2} + \text{contributions from dark matters} \quad (2)$$

For such spherically symmetric spacetime, the modulus of tangent velocity for test particles moving around circular orbits in the equatorial plane can be calculated via [27, 56, 57]

$$v_{\text{tangent}}^2 = \frac{r}{\sqrt{f(r)}} \cdot \frac{d\sqrt{f(r)}}{dr} = r \cdot \frac{d\ln\sqrt{f(r)}}{dr} \quad (3)$$

The analytical form of function  $f(r)$  depends on the dark matter models. Different dark matter models may give different analytical form of function  $f(r)$ , which must be able to give flat rotational curves observed in many galaxies [8, 9]. In the present work, to give a comprehensive study of the dark matter effects on gravitational bending and weak gravitational lensing, we consider dark matter described by perfect fluid with energy-momentum tensor

$$T_{\mu\nu} = (\rho + p)u_\mu u_\nu + pg_{\mu\nu} \quad (4)$$

This is called perfect fluid dark matter (PFDM) in literature [51].

In this work, in order to study the effects of dark matter on gravitational bending and weak gravitational lensing, we choose two renowned classical hole holes in Einstein's general theory of relativity and make them surrounded by PFDM halo. These solutions have been studied many literature, and the effective spacetime metrics have been successfully derived [25, 33, 40, 42, 58, 59].

**Schwarzschild Black Hole Embedded in Perfect Fluid Dark Matter (PFDM):** In the spacetime metric generated by Schwarzschild black hole embedded in PFDM, the function  $f(r)$  can be expressed as:

$$f(r) = 1 - \frac{2M}{r} + \frac{\lambda_{\text{DM}}}{r} \cdot \ln\left(\frac{r}{\lambda_{\text{DM}}}\right) \quad (5)$$

**Charged Reissner-Nordström (RN) Black Hole Embedded in Perfect Fluid Dark Matter (PFDM):** In the spacetime metric generated by charged RN black hole embedded in PFDM halo, the function  $f(r)$  can be expressed as:

$$f(r) = 1 - \frac{2M}{r} + \frac{Q^2}{r^2} + \frac{\lambda_{\text{DM}}}{r} \cdot \ln\left(\frac{r}{\lambda_{\text{DM}}}\right) \quad (6)$$

Here,  $M$  and  $Q$  are the mass and charge of black hole. The  $\lambda_{\text{DM}}$  is the parameter of PFDM, which is proportional to the total effective mass of dark matter halo.

The above spacetime metric (5) and (6) are mostly solved from the Lagrangian

$$\begin{aligned} \mathcal{S} &= \int d^4x \sqrt{-g} \cdot \mathcal{L} \\ &= \int d^4x \sqrt{-g} \cdot \left[ \frac{1}{16\pi G} R + \frac{1}{4} F^{\mu\nu} F_{\mu\nu} + \mathcal{L}_{\text{DM}} \right] \end{aligned} \quad (7)$$

with the energy-momentum tensor of dark matter  $T_{\mu\nu} = (\rho + p)u_\mu u_\nu + pg_{\mu\nu}$ . Furthermore, the density  $\rho$  of PFDM is determined by dark matter parameter  $\lambda_{\text{DM}}$  via [25]

$$\rho = \frac{\lambda_{\text{DM}}}{8\pi r^3} \quad (8)$$

In the PFDM model, to be consistent with the observed galaxy flat rotational curve, the velocity and dark matter parameter should satisfy the relation [28, 58, 60]

$$v^2 = v_{\text{tangent}}^2 \rightarrow \frac{\lambda_{\text{DM}}}{2r_0} \quad (9)$$

where  $v_{\text{tangential}}$  is the modulus of tangent vector for stars traveling along circular orbits in the galaxy, and  $r_0$  is a characteristic distance in the galaxy. In a typical galaxy, when we discussing the gravitational deflection of light and the weak gravitational lensing, it is reasonable to have the following relation [58]

$$r_H \ll b \ll r_0 < r_{\text{halo}} \quad (10)$$

where  $r_H$  is the horizon radius of central supermassive black hole,  $r_{\text{halo}}$  denotes the scale of dark matter halo, and  $b$  is the impact parameter for light beams in gravitational lensing observations.

### III. THEORETICAL FRAMEWORK

This section gives an introduction on the theoretical framework of our work. The subsection III A and subsection III B describes two approaches in calculating the gravitational deflection angle. Subsection III A introduces the Gibbons and Werner approach, in which the gravitational deflection angle is calculated using the Gauss-Bonnet theorem in differential geometry and topology. Subsection III B introduces the conventional geodesic approach, in which the gravitational deflection angle is obtained by solving the trajectories of null geodesics. Subsection III C discusses the photon spheres near black

holes and the shadow radius detected by an observer. Subsection III D is devoted to lens equation and Einstein rings in weak gravitational lensing.

#### A. Gibbons and Werner Approach: the Gauss-Bonnet Theorem and the Gravitational Deflection Angle

According to Einstein's general theory of relativity, the gravitational interaction can be understood as a geometric effect. It is possible to analyze the gravitational bending and gravitational lensing using techniques in geometry and topology. Recently, an approach calculating the gravitational deflection angle of particles utilizing Gauss-Bonnet theorem is emerged. This approach was first introduced by a pioneering work from G. W. Gibbons and M. C. Werner [52], to give a topological interpretation on gravitational deflection. In the later years, this approach has been applied to a number of gravitational systems successfully and consistent results with conventional geodesic methods have been obtained in weak gravitational lensing [61–80].

The Gauss-Bonnet theorem is one of the most profound theorem in differential geometry and topology. It provide nontrivial connections between curvature and topological invariant in a curved manifold. In a two dimensional curved manifold, the mathematical description of Gauss-Bonnet theorem is [81]

$$\int_D \mathcal{K} dS + \int_{\partial D} \kappa_g dl + \sum_{i=1}^N \theta_i = 2\pi\chi(D) \quad (11)$$

Here,  $D$  is a region in curved manifold,  $\mathcal{K}$  is the Gaussian curvature,  $\kappa_g$  is the geodesic curvature of boundary  $\partial D$ ,  $\chi(D)$  is the Euler characteristic number for region  $D$ , and  $\theta_i$  is the exterior angle for each discontinuous point of boundary  $\partial D$ .

In Gibbons and Werner approach, the gravitational deflection angle of massless photon is calculated by applying the Gauss-Bonnet theorem in the optical geometry of black hole spacetime. Similarly, the gravitational deflection angle of massive particle is calculated by applying the Gauss-Bonnet theorem in the Jacobi geometry of black hole spacetime. For static and stationary black holes, the optical geometry can be obtained from the four dimensional black hole spacetime by imposing the null constrain  $d\tau^2 = 0$  [52, 61, 82]

$$\underbrace{d\tau^2 = g_{\mu\nu} dx^\mu dx^\nu}_{\text{Spacetime Geometry}} \stackrel{d\tau^2=0}{\Longrightarrow} \underbrace{dt^2 = g_{ij}^{\text{OP}} dx^i dx^j}_{\text{Optical Geometry}} \quad (12)$$

Particularly, if we consider a four dimensional asymptotically flat and spherically symmetric black hole spacetime

$$\begin{aligned} d\tau^2 &= g_{\mu\nu} dx^\mu dx^\nu \\ &= f(r) dt^2 - \frac{1}{f(r)} dr^2 - r^2(d\theta^2 + r^2 \sin^2 \theta d\phi^2) \end{aligned} \quad (13)$$

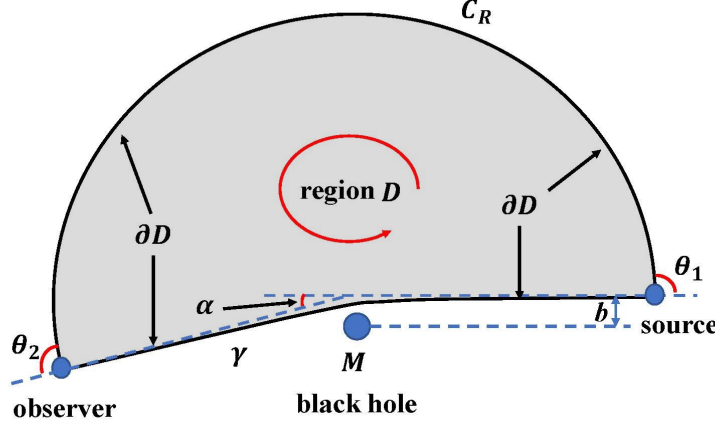


FIG. 1. This figure shows the choice of simply connected region  $D$  in the equatorial plane of optical geometry for asymptotically flat black hole spacetime. In the calculation of gravitational deflection angle, the Gauss-Bonnet theorem in equation (11) is applied for this region. The direction of boundary  $\partial D$  in the contour integral  $\int_{\partial D} \kappa_g dl$  is chosen to be counterclockwise. Note that for particle orbit  $\gamma$ , this choice of direction (which is from observer to light source) is opposite to the propagation of photon beams.

its optical geometry gives a three dimensional Riemannian manifold

$$dt^2 = g_{ij}^{\text{OP}} dx^i dx^j = \frac{1}{f(r)} \left[ \frac{1}{f(r)} dr^2 + r^2 d\theta^2 + r^2 \sin^2 \theta d\phi^2 \right] \quad (14)$$

Since the spacetime is spherical symmetric, without loss of generality, we can restrict the above optical geometry (as well as the optical geometry metric  $g_{ij}^{\text{OP}}$ ) in the equatorial plane. In this way, a two dimensional Riemannian manifold is eventually obtained, and the application of Gauss-Bonnet theorem in equation (11) becomes available.

In the calculations of gravitational deflection angles, one need to choose a region  $D$  in the equatorial plane of optical geometry to apply the Gauss-Bonnet theorem. For asymptotically flat black hole spacetime, when light source and observer are both very far from the central massive black hole,  $D$  is usually chosen to be a simply connected region such that light source and observer are connected by its boundary  $\partial D$ . This boundary is generated by two parts: the particle orbit  $\gamma$  from source to observer, and a circular arc curve  $C_R$ . The central black hole is located outside the region  $D$ , so that spacetime singularities are excluded this region. This region  $D$  is schematically illustrated in figure 1.

For the picked region  $D$  in figure 1, the exterior angles for discontinuous points of boundary  $\partial D$  are  $\theta_1 \approx \theta_2 \approx \pi/2$ . Therefore, in the Gauss-Bonnet theorem, we have the approximation

$$\sum_{i=1}^N \theta_i = \theta_1 + \theta_2 \approx \pi \quad (15)$$

The Euler characteristic number for the simply connected region  $D$  is

$$\chi(D) = 1 \quad (16)$$

Furthermore, in the cases of asymptotically flat black hole spacetime, many studies suggest that the integration of geodesic curvature  $\kappa_g$  along circular arc  $C_R$  in  $R \rightarrow \infty$  limit reduces to [69, 76]

$$\int_{\partial D} \kappa_g dl = \lim_{R \rightarrow \infty} \int_{C_R} \kappa_g(C_R) dl \approx \pi + \alpha \quad (17)$$

where  $\alpha$  is the gravitational deflection angle of light.

Combining the exterior angle in equation (15), Euler characteristic number in equation (16) and contour integral of geodesic curvature in equation (17), the Gauss-Bonnet theorem in equation (11) leads to

$$\begin{aligned} \int_D \mathcal{K} dS + \int_{\partial D} \kappa_g dl + \sum_{i=1}^N \theta_i &= \int_D \mathcal{K} dS + (\pi + \alpha) + \pi \\ &= 2\pi\chi(D) = 2\pi \end{aligned} \quad (18)$$

Eventually, the gravitational deflection angle of light can be calculated through the integration of Gaussian curvature over the picked region  $D$

$$\alpha = - \int_D \mathcal{K} dS \quad (19)$$

From this approach, the gravitational deflection angle is directly linked with geometric and topological properties of optical geometry or black hole. It give us new insights on gravitational bending and weak gravitational lensing.

## B. The Conventional Geodesic Approach to Gravitational Deflection Angle

In the conventional geodesic approach, the gravitational deflection angle is calculated by solving the differential equations of null geodesics. In the past few decades, this approach has been tested by large numbers of observations, and it has become a widely adopted approach in physics and astronomy in both weak and

strong gravitational lensing [83–94].

The key point of conventional geodesic approach is solving the differential equations of null geodesics and computing the variation of azimuthal angle  $\phi$  in the photon trajectory. For spherical symmetric spacetime

$$d\tau^2 = f(r)dt^2 - \frac{1}{f(r)}dr^2 - r^2(d\theta^2 + \sin^2\theta d\phi^2) \quad (20)$$

the geodesic equations can be expressed as [83, 84]

$$\frac{d^2t}{d\lambda^2} + \frac{1}{f(r)} \cdot \frac{df(r)}{dr} \cdot \frac{dt}{d\lambda} \cdot \frac{dr}{d\lambda} = 0 \quad (21a)$$

$$\frac{d^2r}{d\lambda^2} + \frac{f(r)}{2} \cdot \frac{df(r)}{dr} \cdot \left(\frac{dt}{d\lambda}\right)^2 - \frac{1}{2f(r)} \cdot \frac{df(r)}{dr} \cdot \left(\frac{dr}{d\lambda}\right)^2 - r \cdot f(r) \cdot \left(\frac{d\theta}{d\lambda}\right)^2 - r \sin^2\theta \cdot f(r) \cdot \left(\frac{d\phi}{d\lambda}\right)^2 = 0 \quad (21b)$$

$$\frac{d^2\theta}{d\lambda^2} + \frac{2}{r} \cdot \frac{dr}{d\lambda} \cdot \frac{d\theta}{d\lambda} - \sin\theta \cos\theta \cdot \left(\frac{d\phi}{d\lambda}\right)^2 = 0 \quad (21c)$$

$$\frac{d^2\phi}{d\lambda^2} + \frac{2}{r} \cdot \frac{dr}{d\lambda} \cdot \frac{d\phi}{d\lambda} + 2 \cdot \frac{\cos\theta}{\sin\theta} \cdot \frac{d\theta}{d\lambda} \cdot \frac{d\phi}{d\lambda} = 0 \quad (21d)$$

where  $\lambda$  is the affine parameter, and  $B'(r) = dB/dr$ . From the above geodesic equations, two conserved quantities can be obtained [84]

$$J \equiv r^2 \sin^2\theta \frac{d\phi}{d\lambda} = \text{constant} \quad (22a)$$

$$E \equiv f(r) \frac{dt}{d\lambda} = \text{constant} \quad (22b)$$

$$\epsilon \equiv g_{\mu\nu}dx^\mu dx^\nu = f(r) \left( \frac{dt}{d\lambda} \right)^2 - \frac{1}{f(r)} \left( \frac{dr}{d\lambda} \right)^2 - r^2 \left( \frac{d\theta}{d\lambda} \right)^2 - r^2 \sin^2\theta \left( \frac{d\phi}{d\lambda} \right)^2 = \text{constant} \quad (22c)$$

Here,  $J$  is the conserved angular momentum along particle orbit, and  $E^2/2$  can be viewed as the conserved energy along particle orbit. For test particle moving in the equatorial plane  $\theta = \pi/2$ , using these conserved quantities, we obtain the following reduced differential equations

$$\frac{1}{2} \left( \frac{dr}{d\lambda} \right)^2 + \frac{1}{2} f(r) \left[ \frac{J^2}{r^2} + \epsilon \right] = \frac{1}{2} \left( \frac{dr}{d\lambda} \right)^2 + V_{\text{eff}}(r) = \frac{1}{2} E^2 \quad (23a)$$

$$\left( \frac{dr}{d\phi} \right)^2 = \frac{r^4}{b^2} - r^4 \left[ \frac{f(r)}{r^2} + \frac{\epsilon \cdot f(r)}{J^2} \right] \quad (23b)$$

where  $V_{\text{eff}}(r)$  is the effective potential of test particle moving in the spherically symmetric gravitational field. The equation (23b) is derived from equation (23a) using  $d\phi/d\lambda = J/r^2$  and the impact parameter  $b = |J/E|$  for particle orbits in the equatorial plane. For massless (or massive) particles traveling along null (or timelike) geodesics, the value of  $\epsilon$  becomes

$$\begin{aligned} \epsilon &= 0 && \text{particles traveling along null geodesics} \\ \epsilon &= 1 && \text{particles traveling along timelike geodesics} \end{aligned} \quad (24)$$

From the reduced differential equation for particle orbit, we can get

$$\frac{dr}{d\phi} = \pm r^2 \sqrt{\frac{1}{b^2} - \left[ \frac{f(r)}{r^2} + \frac{\epsilon \cdot f(r)}{J^2} \right]} \quad (25)$$

The plus and minus sign  $\pm$  can be determined in the following way. As a test particle moves along the scattering orbit from infinity, the radial coordinate  $r$  decreases and the azimuthal angle  $\phi$  increases, until the test particle reaches the closest distance  $r_0$  to the central supermassive black hole. After the test particle passing the turning point (the

closest distance point), its radial coordinate starts to increase from  $r = r_0$  to  $r = \infty$ , and the azimuthal angle  $\phi$  increases as radius  $r$  increases. In this way, we have the relations

$$\frac{dr}{d\phi} = -r^2 \sqrt{\frac{1}{b^2} - \left[ \frac{f(r)}{r^2} + \frac{\epsilon \cdot f(r)}{J^2} \right]} < 0 \quad \text{particle moving from infinity } r = \infty \text{ to the tuning point } r = r_0 \quad (26a)$$

$$\frac{dr}{d\phi} = r^2 \sqrt{\frac{1}{b^2} - \left[ \frac{f(r)}{r^2} + \frac{\epsilon \cdot f(r)}{J^2} \right]} > 0 \quad \text{particle moving from tuning point } r = r_0 \text{ to infinity } r = \infty \quad (26b)$$

In the gravitational lensing, when light source and observer are both located at infinity, the gravitational deflection angle of light is just twice of the variation  $\Delta\phi$  as radius  $r$  moves from  $r = r_0$  to  $r = \infty$  [84, 85].

$$\begin{aligned} \alpha &= 2|\phi(\infty) - \phi(r_0)| - \pi \\ &= 2 \left| \int_{r_0}^{\infty} \frac{d\phi}{dr} dr \right| - \pi \\ &= 2 \int_{r_0}^{\infty} \frac{dr}{r^2 \sqrt{\frac{1}{b^2} - \frac{f(r)}{r^2}}} - \pi \end{aligned} \quad (27)$$

where  $\epsilon = 0$  has been used for massless photon. From this expression, it is obvious that the gravitational deflection angle  $\alpha$  increases monotonically as the minimal distance  $r_0$  decreases. The turning point  $r = r_0$  must be solved in the integration process. Because  $r_0$  is the closest distance to central black hole, the derivative  $dr/d\lambda$  in equation (23a) vanish

$$\begin{aligned} \frac{dr}{d\lambda} \Big|_{r=r_0} &= 0 \Rightarrow \frac{1}{2} f(r_0) \frac{J^2}{r_0^2} = \frac{1}{2} E^2 \\ &\Rightarrow b^2 = \frac{J^2}{E^2} = \frac{r_0^2}{f(r_0)} \end{aligned} \quad (28)$$

Given a impact parameter for photon orbit, the closest distance  $r_0$  is solved from this equation.

In the numerical calculation, it is useful to find expressions equivalent to (27) and avoid the integration domain reach the  $r = \infty$ . One simple way is adopting  $u = 1/r$  to be the integration variable

$$\alpha = 2 \int_0^{u_0} \frac{du}{\sqrt{\frac{1}{b^2} - f(u) \cdot u^2}} - \pi \quad (29)$$

and  $u_0 = 1/r_0$ . Another way is assigning the  $x = r_0/r$  to be integration variable

$$\begin{aligned} \alpha &= 2 \int_{r_0}^{\infty} \frac{dr}{r^2 \sqrt{\frac{1}{b^2} - \frac{f(r)}{r^2}}} - \pi \\ &= 2 \int_{r_0}^{\infty} \frac{dr}{r^2 \sqrt{\frac{f(r_0)}{r_0^2} - \frac{f(r)}{r^2}}} - \pi \\ &= 2 \int_{r_0}^{\infty} \frac{r_0 dr}{r^2 \sqrt{f(r_0) - \left(\frac{r_0}{r}\right)^2 \cdot f(r)}} - \pi \\ &= 2 \int_0^1 \frac{dx}{\sqrt{F_0 - F(x)}} - \pi \end{aligned} \quad (30)$$

where  $F_0$  and  $F(x)$  is defined through

$$F(x) \equiv x^2 \cdot f(r) = x^2 \cdot f\left(\frac{r_0}{x}\right) \quad (31a)$$

$$F_0 \equiv f(r_0) = F(x = 1) \quad (31b)$$

In the presented work, we choose the equation (30) to carry out the numerical integration.

### C. Photon Sphere and Black Hole Shadow

The photon spheres and black hole shadows are crucial quantities in the gravitational lensing. These quantities reflect many intrinsic properties of black holes and other massive compact objects. Recently, the black hole shadow image in the center M87 galaxy and Sgr A\* caught by Event Horizon Telescope (EHT) stimulated large numbers of investigations on black holes and gravitational lensing.

Conventionally, the exact positions of photon spheres near black hole are achieved using the effective potentials of test particles (photons) [83, 95–100]. For static and spherically-symmetric black holes in equation (20), the photon equation of motion has a simple form

$$\frac{1}{2} \cdot \frac{d^2r}{d\lambda^2} + V_{\text{eff}}(r) = \frac{1}{2} \cdot E^2 \quad (32)$$

with the photon effective potential

$$V_{\text{eff}}(r) = \frac{f(r)}{2} \cdot \frac{J^2}{r^2} \quad (33)$$

The local maximal points of effective potential give the unstable photon spheres, while the local minimal points of effective potential give the unstable photon spheres near black holes.

$$\begin{aligned} \frac{dV_{\text{eff}}(r)}{dr} &= 0 \Leftrightarrow \text{photon sphere} \\ \frac{dV_{\text{eff}}(r)}{dr} &= 0 \quad \text{and} \quad \frac{d^2V_{\text{eff}}(r)}{dr^2} < 0 \Leftrightarrow \text{unstable photon sphere} \\ \frac{dV_{\text{eff}}(r)}{dr} &= 0 \quad \text{and} \quad \frac{d^2V_{\text{eff}}(r)}{dr^2} > 0 \Leftrightarrow \text{stable photon sphere} \end{aligned} \quad (34)$$

Recently, a new geometric approach is proposed such that the stable and unstable photon spheres are determined

by the Gaussian curvature and geodesic curvature introduced in subsection III A. In this geometric approach, the positions of photon spheres are acquired using the optical geometry [53, 54]. The photon spheres are circles in optical geometry with zero geodesic curvature  $\kappa_g(r) = 0$ . In addition, the negative Gaussian curvature in equatorial plane of optical geometry indicates the corresponding

photon spheres (where  $\kappa_g(r) = 0$  and  $\mathcal{K}(r) < 0$ ) are unstable, while the positive Gaussian curvature indicates the photon spheres (where  $\kappa_g(r) = 0$  and  $\mathcal{K}(r) > 0$ ) are stable. Furthermore, it is also proved that the above geometric approach is completely equivalent to the conventional approach using the effective potential of test particles.

$$\frac{dV_{\text{eff}}(r)}{dr} \Big|_{r=r_{ph}} = 0 \Leftrightarrow \left\{ \frac{J^2}{r^2} \cdot \left[ \frac{1}{2} \cdot \frac{df(r)}{dr} - \frac{f(r)}{r} \right] \right\}_{r=r_{ph}} = 0 \Leftrightarrow \kappa_g(r = r_{ph}) = 0 \quad (35a)$$

$$\frac{d^2V_{\text{eff}}(r)}{dr^2} \Big|_{r=r_{ph}} < 0 \Leftrightarrow \left\{ \frac{J^2}{2r^2} \cdot \left[ \frac{f(r)}{2} \cdot \frac{d^2f(r)}{dr^2} - \left( \frac{1}{2} \cdot \frac{df(r)}{dr} \right)^2 \right] \right\}_{r=r_{ph}} < 0 \Leftrightarrow \mathcal{K}(r) \Big|_{r=r_{ph}} > 0 \quad (35b)$$

$$\frac{d^2V_{\text{eff}}(r)}{dr^2} \Big|_{r=r_{ph}} > 0 \Leftrightarrow \left\{ \frac{J^2}{2r^2} \cdot \left[ \frac{f(r)}{2} \cdot \frac{d^2f(r)}{dr^2} - \left( \frac{1}{2} \cdot \frac{df(r)}{dr} \right)^2 \right] \right\}_{r=r_{ph}} > 0 \Leftrightarrow \mathcal{K}(r) \Big|_{r=r_{ph}} > 0 \quad (35c)$$

Black hole shadows are closely connected with the unstable photon spheres. For a static spherically-symmetric black hole, an observer far away from the black hole would observe the following angular radius of black hole shadow [99]

$$\sin^2 \alpha_{sh} = \frac{h(r_{ph})^2}{h(r_{\text{obs}})^2} = \frac{b_{\text{critical}}^2}{h(r_{\text{obs}})^2} \quad (36)$$

where  $r_{\text{obs}}$  is the distance between observer and central black hole, and  $h(r)$  is defined by

$$h(r) \equiv \sqrt{\frac{g_{\phi\phi}(r, \theta = \frac{\pi}{2})}{-g_{tt}(r)}} = \frac{r}{\sqrt{f(r)}} \quad (37)$$

Meanwhile, the critical impact parameter can also give a absolute size / radius of the black hole shadow.

$$r_{sh} = b_{\text{critical}} = \frac{r_{ph}}{\sqrt{f(r_{ph})}} \quad (38)$$

This is the analytical expression of black hole shadow radius for spherically symmetric black hole detected by observer located at infinity [99].

#### D. Lens Equation and Einstein Ring in the Weak Gravitational Lensing

In gravitational lensing observations, physical observables are mostly constrained by lens equation. Other quantities, such as the position of lensed objects, as well as the Einstein ring, can be calculated by solving the lens

equation. There are a number of gravitational lens equation in the past decades [85, 86, 90, 101–105]. Here, we use a famous lens equation given by V. Bozza [90]

$$D_{\text{OS}} \tan \beta = \frac{D_{\text{OL}} \sin \theta - D_{\text{LS}} \sin(\alpha - \theta)}{\cos(\alpha - \theta)} \quad (39)$$

Here,  $D_{\text{OS}}$  is the distance between observer and source plane,  $D_{\text{OL}}$  is the distance between observer and lens plane,  $D_{\text{LS}}$  is the distance between lens plane and source plane. The angle  $\beta$  in equation (39) denotes the “exact” angular position of the luminous light source, while the angle  $\theta$  is the visual angular position of the lensed image seen by an observer faraway. The images of the lensed objects (which are luminous heavenly bodies) can be achieved by solving lens equation (39). In the weak gravitational lensing cases, for distant source and observer, we have the approximations  $\tan \beta \approx \beta$ ,  $\sin \theta \approx \theta$  and  $\sin(\alpha - \theta) \approx \alpha - \theta$ . Then the lens equation (39) reduces to the following form [48, 103]

$$\beta = \theta - \frac{D_{\text{LS}}}{D_{\text{OS}}} \cdot \alpha \quad (40)$$

The relation  $D_{\text{OS}} = D_{\text{OL}} + D_{\text{LS}}$  has been used to derive this equation. The angular radius of Einstein ring is calculated by taking  $\beta = 0$ .

$$\theta_{\text{E}} = \frac{D_{\text{LS}}}{D_{\text{OS}}} \cdot \alpha \quad (41)$$

Further, in the weak gravitational lensing case, the impact parameter  $b$  satisfies

$$b \approx D_{\text{OL}} \sin \theta_{\text{E}} \approx D_{\text{OL}} \theta_{\text{E}} \quad (42)$$

Once the expression of gravitational deflection angle  $\alpha$  is known, the angular radius of Einstein ring  $\theta_{\text{E}}$  can be solved by combing equation (41) and equation (42).

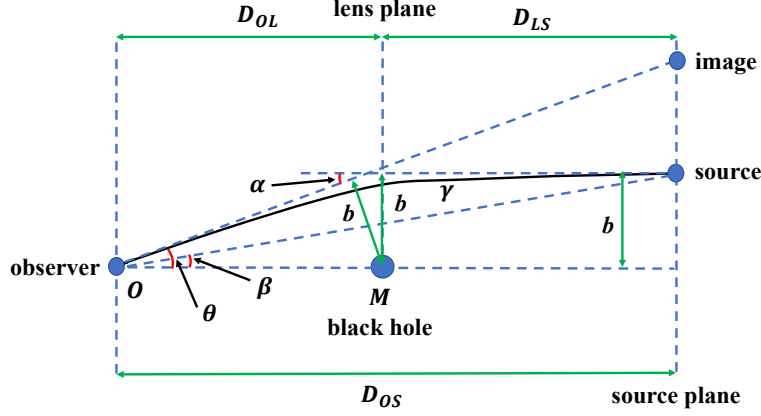


FIG. 2. Schematically plot of the weak gravitation lensing. The photon emitted by light source (luminous heavenly bodies) is lensed by the central supermassive black hole. In this figure,  $D_{OS}$  is the distance between observer and source plane,  $D_{OL}$  is the distance between observer and lens plane,  $D_{LS}$  is the distance between lens plane and source plane. The central black hole is in the middle of lens plane. The angle  $\beta$  denotes the angular position of light source with respect to axis  $OM$ , and  $\theta$  is the angular position of the lensed image seen by an observer. The  $\alpha$  is the gravitational deflection angle of light, and  $b$  is the impact parameter.

#### IV. GRAVITATIONAL DEFLECTION ANGLES OF LIGHT

This section present the gravitational deflection angle of light near a supermassive black hole embedded in perfect fluid dark matter (PFDM). The subsection IV A presents the analytical results obtained in Gibbons and Werner approach by applying the Gauss-Bonnet theorem in the optical geometry of black hole spacetime .The subsection IV B displays the results obtained using the conventional geodesic approach, where the gravitational deflection angles of light for Schwarzschild and charged Reissner-Nordström (RN) black holes embedded in PFDM are calculated by solving the trajectories of photon orbits.

##### A. Results from the Gibbons and Werner Approach (Gauss-Bonnet theorem)

###### Schwarzschild Black Hole Embedded in Perfect Fluid Dark Matter (PFDM):

In the Gibbons and Werner approach, the gravitational deflection angle is calculated by a surface integral of Gaussian curvature in equation (19). For Schwarzschild black hole embedded in PFDM, the corresponding optical geometry restricted in the equatorial plane ( $\theta = \pi/2$ ) is

$$dt^2 = \tilde{g}_{ij}^{\text{OP}} dx^i dx^j = \frac{1}{[f(r)]^2} dr^2 + \frac{r^2}{f(r)} d\phi^2 = \frac{dr^2}{[1 - \frac{2M}{r} + \frac{\lambda_{\text{DM}}}{r} \cdot \ln(\frac{r}{\lambda_{\text{DM}}})]^2} + \frac{r^2 d\phi^2}{1 - \frac{2M}{r} + \frac{\lambda_{\text{DM}}}{r} \cdot \ln(\frac{r}{\lambda_{\text{DM}}})} \quad (43)$$

The Gaussian curvature in the equatorial plane of optical manifold can be expressed as [106]

$$\mathcal{K}(r) = -\frac{1}{\sqrt{\tilde{g}^{\text{OP}}}} \left[ \partial_\phi \left( \frac{\partial_\phi(\sqrt{\tilde{g}_{rr}^{\text{OP}}})}{\sqrt{\tilde{g}_{\phi\phi}^{\text{OP}}}} \right) + \partial_r \left( \frac{\partial_r(\sqrt{\tilde{g}_{\phi\phi}^{\text{OP}}})}{\sqrt{\tilde{g}_{rr}^{\text{OP}}}} \right) \right] \quad (44)$$

$$\begin{aligned} &= \frac{1}{2} f(r) \cdot \frac{d^2 f(r)}{dr^2} - \left[ \frac{1}{2} \cdot \frac{df(r)}{dr} \right]^2 \\ &= -\frac{4M + 3\lambda_{\text{DM}}}{2r^3} + \frac{12M^2 + 8M\lambda_{\text{DM}} - \lambda_{\text{DM}}^2}{4r^4} + \left[ \frac{\lambda_{\text{DM}}}{r^3} - \frac{\lambda_{\text{DM}}^2 + 3M\lambda_{\text{DM}}}{r^4} \right] \cdot \ln\left(\frac{r}{\lambda_{\text{DM}}}\right) + \frac{3\lambda_{\text{DM}}^2}{4r^4} \cdot \left[ \ln\left(\frac{r}{\lambda_{\text{DM}}}\right) \right]^2 \end{aligned} \quad (45)$$

and the surface area in the equatorial plane can be calculated through

$$\begin{aligned} dS &= \sqrt{\tilde{g}^{\text{OP}}} dr d\phi = \frac{r}{[f(r)]^{3/2}} dr d\phi \\ &= \left\{ 1 + \frac{3M}{r} - \frac{3\lambda_{\text{DM}}}{2r} \cdot \ln\left(\frac{r}{\lambda_{\text{DM}}}\right) + \frac{15[2M - \lambda_{\text{DM}} \cdot \ln(\frac{r}{\lambda_{\text{DM}}})]^2}{8r^2} + \text{higher orders} \right\} r dr d\phi \end{aligned} \quad (46)$$

In the optical geometry, the geodesic curvature  $\kappa_g$  of outer circular arc  $C_R$  is calculated as follows [106]

$$\kappa_g(C_R) = \frac{1}{2\sqrt{\tilde{g}_{rr}^{\text{OP}}}} \frac{\partial \ln \tilde{g}_{\phi\phi}^{\text{OP}}}{\partial r} \Big|_{r=R} = \left[ \frac{f(r)}{r} - \frac{1}{2} \frac{\partial f(r)}{\partial r} \right]_{r=R} = \frac{1}{R} - \frac{6M + \lambda_{\text{DM}}}{2R^2} + \frac{3\lambda_{\text{DM}}}{2R^2} \cdot \ln\left(\frac{R}{\lambda_{\text{DM}}}\right) \quad (47)$$

For Schwarzschild black hole embedded in PFDM medium, it can be easily seen that the corresponding optical geometry is a asymptotically flat space, because the Gaussian curvature and geodesic converge in equations (45) and (47) approach to zero in the  $r \rightarrow \infty$  (or  $R \rightarrow \infty$ ) limit. Base on the asymptotically flat property of the optical geometry (the geodesic curvature of outer circular arc approaches to  $\kappa_g(C_R) \rightarrow 1/R$  when  $R \rightarrow \infty$ ), the contour integration of geodesic curvature  $\kappa_g$  along the boundary  $\partial D$  becomes

$$\begin{aligned} \int_{\partial D} \kappa_g dl &= \lim_{R \rightarrow \infty} \int_{C_R} \kappa_g(C_R) \cdot dl = \lim_{R \rightarrow \infty} \int_{\phi_{\text{source}}}^{\phi_{\text{observer}}} \kappa_g(C_R) \cdot R d\phi \\ &\approx \lim_{R \rightarrow \infty} \int_0^{\pi+\alpha} \left[ \frac{1}{R} - \frac{6M + \lambda_{\text{DM}}}{2R^2} + \frac{3\lambda_{\text{DM}}}{2R^2} \cdot \ln\left(\frac{R}{\lambda_{\text{DM}}}\right) \right] R d\phi \\ &= \pi + \alpha \end{aligned} \quad (48)$$

which is consistent with the contour integral for asymptotically flat spacetime in equation (17). In the calculation of contour integral, we assume that the gravitational deflection angle is not large, which correspond to the weak gravitational lensing observations. In this case, we have the approximation  $\phi_{\text{source}} \approx 0$  and  $\phi_{\text{observer}} \approx \pi + \alpha \approx \pi$  for azimuthal angles.

The gravitational deflection angle of light for Schwarzschild black hole embedded in PFDM halo is obtained from the integration of Gaussian curvature over the picked region  $D$  in figure 1.

$$\begin{aligned} \alpha &= - \int_D \mathcal{K}(r) \cdot dS \\ &= - \int_{\phi_{\text{source}}}^{\phi_{\text{observer}}} d\phi \int_{r(\gamma)}^{\infty} \mathcal{K}(r) \cdot \frac{r}{[f(r)]^{3/2}} dr \approx - \int_0^{\pi} d\phi \int_{\frac{b}{\sin \phi}}^{\infty} \mathcal{K}(r) \cdot \frac{r}{[f(r)]^{3/2}} dr \\ &= - \int_0^{\pi} d\phi \int_{\frac{b}{\sin \phi}}^{\infty} \left\{ -\frac{4M + 3\lambda_{\text{DM}}}{2r^2} + \frac{\lambda_{\text{DM}}}{r^2} \cdot \ln\left(\frac{r}{\lambda_{\text{DM}}}\right) - \frac{12M^2 + 10M\lambda_{\text{DM}} + \lambda_{\text{DM}}^2}{4r^3} \right. \\ &\quad \left. + \frac{12M\lambda_{\text{DM}} + 5\lambda_{\text{DM}}^2}{4r^3} \cdot \ln\left(\frac{r}{\lambda_{\text{DM}}}\right) - \frac{3\lambda_{\text{DM}}^2}{4r^3} \cdot \left[ \ln\left(\frac{r}{\lambda_{\text{DM}}}\right) \right]^2 \right\} dr + \text{higher orders} \\ &= \int_0^{\pi} d\phi \cdot \left\{ \frac{(4M + 3\lambda_{\text{DM}}) \cdot \sin \phi}{2b} - \frac{\lambda_{\text{DM}} \cdot \sin \phi}{b} \cdot \left[ \ln\left(\frac{b}{\lambda_{\text{DM}} \cdot \sin \phi}\right) + 1 \right] \right. \\ &\quad \left. + \frac{(12M^2 + 10M\lambda_{\text{DM}} + \lambda_{\text{DM}}^2) \cdot \sin^2 \phi}{8b^2} - \frac{12M\lambda_{\text{DM}} + 5\lambda_{\text{DM}}^2}{4} \cdot \left[ \frac{\sin^2 \phi}{2b^2} \cdot \ln\left(\frac{b}{\lambda_{\text{DM}} \cdot \sin \phi}\right) + \frac{\sin^2 \phi}{4b^2} \right] \right. \\ &\quad \left. + \frac{3\lambda_{\text{DM}}^2}{4} \cdot \left[ \frac{\sin^2 \phi}{2b^2} \cdot \left( \ln\left(\frac{b}{\lambda_{\text{DM}} \cdot \sin \phi}\right) \right)^2 + \frac{\sin^2 \phi}{2b^2} \cdot \ln\left(\frac{b}{\lambda_{\text{DM}} \cdot \sin \phi}\right) + \frac{\sin^2 \phi}{4b^2} \right] \right\} + \text{higher orders} \\ &= \frac{4M - \lambda_{\text{DM}}}{b} - \frac{2\lambda_{\text{DM}}}{b} \cdot \ln\left(\frac{b}{2\lambda_{\text{DM}}}\right) + \frac{(12M^2 + 10M\lambda_{\text{DM}} + \lambda_{\text{DM}}^2) \cdot \pi}{16b^2} + \frac{\pi\lambda_{\text{DM}}^2}{12b^2} \cdot \left[ \frac{\pi^2}{12} - \frac{1}{2} \right] \\ &\quad - \frac{(12M\lambda_{\text{DM}} + 5\lambda_{\text{DM}}^2) \cdot \pi}{16b^2} \cdot \ln\left(\frac{2b}{\lambda_{\text{DM}}}\right) + \frac{3\pi\lambda_{\text{DM}}^2}{16b^2} \cdot \left[ \ln\left(\frac{2b}{\lambda_{\text{DM}}}\right) \right]^2 + \text{higher orders} \end{aligned} \quad (49)$$

The higher orders terms include the terms  $\frac{M^3}{b^3}$ ,  $\frac{M^2\lambda_{\text{DM}}}{b^3}$ ,  $\frac{M\lambda_{\text{DM}}^2}{b^3}$ ,  $\frac{\lambda_{\text{DM}}^3}{b^3}$ ,  $\frac{M^2\lambda_{\text{DM}}}{b^3} \ln(\frac{b}{\lambda_{\text{DM}}})$ ,  $\frac{M\lambda_{\text{DM}}^2}{b^3} \ln(\frac{b}{\lambda_{\text{DM}}})$ ,  $\frac{\lambda_{\text{DM}}^3}{b^3} \ln(\frac{b}{\lambda_{\text{DM}}})$ ,  $\frac{M\lambda_{\text{DM}}^2}{b^3} [\ln(\frac{b}{\lambda_{\text{DM}}})]^2$ ,  $\frac{\lambda_{\text{DM}}^3}{b^3} [\ln(\frac{b}{\lambda_{\text{DM}}})]^2$ ,  $\frac{\lambda_{\text{DM}}^3}{b^3} [\ln(\frac{b}{\lambda_{\text{DM}}})]^3$ , which would be very complicated. In the above integration process, the radius of photon orbit  $r(\gamma) = r(\phi)$  in the lower bound of integral should be known. In Gibbons and

Werner approach, it is not necessary to solve the photon orbit directly, and  $r(\phi)$  in the lower bound of integral often replaced by an approximate solution, to avoid solving any complicated differential equations for particle orbits. Here, we use the leading order perturbation  $r(\gamma) = r(\phi) \approx b/\sin \phi$  in the analytical integration, where  $b$  is impact parameter indicated in figure 1. The result in equation (49) agrees with the gravitational deflection angle derived by S. Haroon. In 2019, S. Haroon *et al.* gives a leading order contribution of deflection angle for rotating black holes embedded in PFDM [33]

$$\alpha = \frac{4M}{b} - \frac{\lambda_{\text{DM}}}{b} \cdot \left[ 1 - 2 \ln 2 + 2 \ln \left( \frac{b}{\lambda_{\text{DM}}} \right) \right] \pm \frac{4aM}{b^2} \quad (50)$$

The  $a = 0$  corresponds to the non-rotating Schwarzschild black hole embedded in PFDM, which is perfectly identical to our calculation. In this way, our result can be viewed as an extension of Haroon's result to the next-to-leading order (the  $\frac{M^2}{b^2}$ ,  $\frac{M\lambda_{\text{DM}}}{b^2}$ ,  $\frac{\lambda_{\text{DM}}^2}{b^2}$ ,  $\frac{M\lambda_{\text{DM}}}{b^2} \ln \left( \frac{b}{\lambda_{\text{DM}}} \right)$ ,  $\frac{\lambda_{\text{DM}}^2}{b^2} \ln \left( \frac{b}{\lambda_{\text{DM}}} \right)$ ,  $\frac{\lambda_{\text{DM}}^2}{b^2} \left[ \ln \left( \frac{b}{\lambda_{\text{DM}}} \right) \right]^2$  terms).

### Charged Reissner-Nordström (RN) Black Hole Embedded in Perfect Fluid Dark Matter (PFDM):

For charged RN black hole embedded in PFDM, the optical geometry restricted in equatorial plane ( $\theta = \pi/2$ ) gives

$$\begin{aligned} dt^2 = \tilde{g}_{ij}^{\text{OP}} dx^i dx^j &= \frac{1}{[f(r)]^2} dr^2 + \frac{r^2}{f(r)} d\phi^2 \\ &= \frac{dr^2}{\left[ 1 - \frac{2M}{r} + \frac{Q^2}{r^2} + \frac{\lambda_{\text{DM}}}{r} \cdot \ln \left( \frac{r}{\lambda_{\text{DM}}} \right) \right]^2} + \frac{r^2 d\phi^2}{1 - \frac{2M}{r} + \frac{Q^2}{r^2} + \frac{\lambda_{\text{DM}}}{r} \cdot \ln \left( \frac{r}{\lambda_{\text{DM}}} \right)} \end{aligned} \quad (51)$$

The Gaussian curvature in the equatorial plane of optical manifold can be expressed as

$$\begin{aligned} \mathcal{K}(r) &= -\frac{1}{\sqrt{\tilde{g}^{\text{OP}}}} \left[ \partial_\phi \left( \frac{\partial_\phi(\sqrt{\tilde{g}_{rr}^{\text{OP}}})}{\sqrt{\tilde{g}_{\phi\phi}^{\text{OP}}}} \right) + \partial_r \left( \frac{\partial_r(\sqrt{\tilde{g}_{\phi\phi}^{\text{OP}}})}{\sqrt{\tilde{g}_{rr}^{\text{OP}}}} \right) \right] \\ &= \frac{1}{2} f(r) \cdot \frac{d^2 f(r)}{dr^2} - \left[ \frac{1}{2} \cdot \frac{df(r)}{dr} \right]^2 \\ &= -\frac{4M + 3\lambda_{\text{DM}}}{2r^3} + \frac{12(M^2 + Q^2) + 8M\lambda_{\text{DM}} - \lambda_{\text{DM}}^2}{4r^4} - \frac{12MQ^2 + Q^2\lambda_{\text{DM}}}{2r^5} + \frac{2Q^4}{r^6} \\ &\quad + \left[ \frac{\lambda_{\text{DM}}}{r^3} - \frac{\lambda_{\text{DM}}^2 + 3M\lambda_{\text{DM}}}{r^4} + \frac{3Q^2\lambda_{\text{DM}}}{r^5} \right] \cdot \ln \left( \frac{r}{\lambda_{\text{DM}}} \right) + \frac{3\lambda_{\text{DM}}^2}{4r^4} \cdot \left[ \ln \left( \frac{r}{\lambda_{\text{DM}}} \right) \right]^2 \end{aligned} \quad (52)$$

And the surface area in the equatorial plane can be expressed as

$$\begin{aligned} dS &= \sqrt{\tilde{g}^{\text{OP}}} dr d\phi = \frac{r}{[f(r)]^{3/2}} dr d\phi \\ &= \left\{ 1 + \frac{3M}{r} - \frac{3\lambda_{\text{DM}}}{2r} \cdot \ln \left( \frac{r}{\lambda_{\text{DM}}} \right) + \frac{3Q^2}{2r^2} + \frac{15[2M - \lambda_{\text{DM}} \cdot \ln(\lambda_{\text{DM}})]^2}{8r^2} + \text{higher orders} \right\} r dr d\phi \end{aligned} \quad (53)$$

The geodesic curvature  $\kappa_g$  of outer circular arc  $C_R$  can be calculated from the following expression

$$\kappa_g(C_R) = \frac{1}{2\sqrt{\tilde{g}_{rr}^{\text{OP}}}} \frac{\partial \ln \tilde{g}_{\phi\phi}^{\text{OP}}}{\partial r} \Big|_{r=R} = \left[ \frac{f(r)}{r} - \frac{1}{2} \frac{\partial f(r)}{\partial r} \right]_{r=R} = \frac{1}{R} - \frac{6M + \lambda_{\text{DM}}}{2R^2} + \frac{3\lambda_{\text{DM}}}{2R^2} \cdot \ln \left( \frac{R}{\lambda_{\text{DM}}} \right) + \frac{2Q^2}{R^3} \quad (54)$$

For charged RN black hole embedded in PFDM medium, the optical geometry is also a asymptotically flat space, and the Gaussian curvature and geodesic converge in equations (52) and (54) approach to zero in the  $r \rightarrow \infty$  limit. Then integration of geodesic curvature  $\kappa_g$  along the boundary  $\partial D$  becomes

$$\begin{aligned} \int_{\partial D} \kappa_g dl &= \lim_{R \rightarrow \infty} \int_{C_R} \kappa_g(C_R) \cdot dl = \lim_{R \rightarrow \infty} \int_{\phi_{\text{source}}}^{\phi_{\text{observer}}} \kappa_g(C_R) \cdot R d\phi \\ &\approx \lim_{R \rightarrow \infty} \int_0^{\pi+\alpha} \left[ \frac{1}{R} - \frac{6M + \lambda_{\text{DM}}}{2R^2} + \frac{3\lambda_{\text{DM}}}{2R^2} \cdot \ln \left( \frac{R}{\lambda_{\text{DM}}} \right) + \frac{2Q^2}{R^3} \right] R d\phi \\ &= \pi + \alpha \end{aligned} \quad (55)$$

Similar to the Schwarzschild black hole embedded in PFDM, the boundary contour integral for RN black hole embedded in PFDM is consistent with the asymptotically flat spacetime result in equation (17). In the weak

gravitational lensing where the gravitational deflection angle is not large, it is possible to use the approximation  $\phi_{\text{source}} \approx 0$  and  $\phi_{\text{observer}} \approx \pi + \alpha \approx \pi$  for azimuthal angles. Furthermore, if we use the leading order approximation  $r(\gamma) = r(\phi) \approx b/\sin \phi$  for photon orbit in the lower bound of the integral of Gaussian curvature, the gravitational deflection angle of light for charged RN black hole embedded in PFDM can be obtained

$$\begin{aligned}
\alpha &= - \int_D \mathcal{K}(r) \cdot dS \\
&\approx - \int_0^\pi d\phi \int_{\frac{b}{\sin \phi}}^\infty \mathcal{K}(r) \cdot \frac{r}{[f(r)]^{3/2}} dr \\
&= - \int_0^\pi d\phi \int_{\frac{b}{\sin \phi}}^\infty \left\{ -\frac{4M + 3\lambda_{\text{DM}}}{2r^2} + \frac{\lambda_{\text{DM}}}{r^2} \cdot \ln \left( \frac{r}{\lambda_{\text{DM}}} \right) - \frac{12(M^2 - Q^2) + 10M\lambda_{\text{DM}} + \lambda_{\text{DM}}^2}{4r^3} \right. \\
&\quad \left. + \frac{12M\lambda_{\text{DM}} + 5\lambda_{\text{DM}}^2}{4r^3} \cdot \ln \left( \frac{r}{\lambda_{\text{DM}}} \right) - \frac{3\lambda_{\text{DM}}^2}{4r^3} \cdot \left[ \ln \left( \frac{r}{\lambda_{\text{DM}}} \right) \right]^2 \right\} dr + \text{higher orders} \\
&= \int_0^\pi d\phi \cdot \left\{ \frac{(4M + 3\lambda_{\text{DM}}) \cdot \sin \phi}{2b} - \frac{\lambda_{\text{DM}} \cdot \sin \phi}{b} \cdot \left[ \ln \left( \frac{b}{\lambda_{\text{DM}} \cdot \sin \phi} \right) + 1 \right] \right. \\
&\quad \left. + \frac{(12M^2 - 12Q^2 + 10M\lambda_{\text{DM}} + \lambda_{\text{DM}}^2) \cdot \sin^2 \phi}{8b^2} \right. \\
&\quad \left. - \frac{12M\lambda_{\text{DM}} + 5\lambda_{\text{DM}}^2}{4} \cdot \left[ \frac{\sin^2 \phi}{2b^2} \cdot \ln \left( \frac{b}{\lambda_{\text{DM}} \cdot \sin \phi} \right) + \frac{\sin^2 \phi}{4b^2} \right] \right. \\
&\quad \left. + \frac{3\lambda_{\text{DM}}^2}{4} \cdot \left[ \frac{\sin^2 \phi}{2b^2} \cdot \left( \ln \left( \frac{b}{\lambda_{\text{DM}} \cdot \sin \phi} \right) \right)^2 + \frac{\sin^2 \phi}{2b^2} \cdot \ln \left( \frac{b}{\lambda_{\text{DM}} \cdot \sin \phi} \right) + \frac{\sin^2 \phi}{4b^2} \right] \right\} + \text{higher orders} \\
&= \frac{4M - \lambda_{\text{DM}}}{b} - \frac{2\lambda_{\text{DM}}}{b} \cdot \ln \left( \frac{b}{2\lambda_{\text{DM}}} \right) + \frac{(12M^2 - 12Q^2 + 10M\lambda_{\text{DM}} + \lambda_{\text{DM}}^2) \cdot \pi}{16b^2} + \frac{3\pi\lambda_{\text{DM}}^2}{16b^2} \cdot \left[ \frac{\pi^2}{12} - \frac{1}{2} \right] \\
&\quad - \frac{(12M\lambda_{\text{DM}} + 5\lambda_{\text{DM}}^2) \cdot \pi}{16b^2} \cdot \ln \left( \frac{2b}{\lambda_{\text{DM}}} \right) + \frac{3\pi\lambda_{\text{DM}}^2}{16b^2} \cdot \left[ \ln \left( \frac{2b}{\lambda_{\text{DM}}} \right) \right]^2 + \text{higher orders} \tag{56}
\end{aligned}$$

The higher orders terms include the terms  $\frac{M^3}{b^3}$ ,  $\frac{MQ^2}{b^3}$ ,  $\frac{M^2\lambda_{\text{DM}}}{b^3}$ ,  $\frac{Q^2\lambda_{\text{DM}}}{b^3}$ ,  $\frac{M\lambda_{\text{DM}}^2}{b^3}$ ,  $\frac{\lambda_{\text{DM}}^3}{b^3}$ ,  $\frac{M^2\lambda_{\text{DM}}}{b^3} \ln(\frac{b}{\lambda_{\text{DM}}})$ ,  $\frac{Q^2\lambda_{\text{DM}}}{b^3} \ln(\frac{b}{\lambda_{\text{DM}}})$ ,  $\frac{M\lambda_{\text{DM}}^2}{b^3} \ln(\frac{b}{\lambda_{\text{DM}}})$ ,  $\frac{\lambda_{\text{DM}}^3}{b^3} \ln(\frac{b}{\lambda_{\text{DM}}})$ ,  $\frac{M\lambda_{\text{DM}}^2}{b^3} \left[ \ln(\frac{b}{\lambda_{\text{DM}}}) \right]^2$ ,  $\frac{\lambda_{\text{DM}}^3}{b^3} \left[ \ln(\frac{b}{\lambda_{\text{DM}}}) \right]^2$ ,  $\frac{\lambda_{\text{DM}}^3}{b^3} \left[ \ln(\frac{b}{\lambda_{\text{DM}}}) \right]^3$ . The gravitational deflection angle of light calculated in equation (56) is consistent with the result given by F. Atamurotov *et al.* in reference [38]

$$\alpha = \frac{2M}{b} \left( 1 + \frac{1}{v^2} \right) - \frac{\pi Q^2}{4b^2} \left( 1 + \frac{2}{v^2} \right) + \frac{\lambda_{\text{DM}}}{v^2 b} \left[ (1 + v^2) \ln 2 - (1 + v^2) \ln \left( \frac{b}{\lambda_{\text{DM}}} \right) - v^2 \right] \pm \frac{4aM}{b^2 v} \tag{57}$$

with  $v = 1$  for massless photon and  $a = 0$  for non-rotating charged black hole embedded in PFDM. Atamurotov only gives the contribution from black hole charge in the next-to-leading order (the  $\frac{Q^2}{b^2}$  term). Our work present the black hole mass and dark matter contributions to gravitational deflection angle in the next-to-leading order (include the  $\frac{M^2}{b^2}$ ,  $\frac{M\lambda_{\text{DM}}}{b^2}$ ,  $\frac{\lambda_{\text{DM}}^2}{b^2}$ ,  $\frac{M\lambda_{\text{DM}}}{b^2} \ln(\frac{b}{\lambda_{\text{DM}}})$ ,  $\frac{\lambda_{\text{DM}}^2}{b^2} \ln(\frac{b}{\lambda_{\text{DM}}})$ ,  $\frac{\lambda_{\text{DM}}^2}{b^2} \left[ \ln(\frac{b}{\lambda_{\text{DM}}}) \right]^2$  terms). Particularly, in the absence of dark matter halo  $\lambda = 0$ , the gravitational deflection angle of light becomes  $\alpha \approx 4M/b + (3M^2 - 3Q^2) \cdot \pi/4b^2$ .

## B. Results From the Conventional Geodesic Approach

In the conventional geodesic approach, the gravitational deflection light is calculated by solving the trajectory of photon orbit near black hole. Following the algorithm presented in subsection III B, the gravitational deflection angle of light can be obtained from the change of azimuthal angle  $\Delta\phi$ . In this work, we utilize the expression (30) to calculate the gravitational deflection an-

gle of light for infinity source and observers.

$$\alpha = 2 \int_0^1 \frac{dx}{\sqrt{F_0 - F(x)}} - \pi \tag{58}$$

For Schwarzschild black hole embedded in PFDM, the explicit expression for  $F_0$  and  $F(x)$  are

$$F(x) = x^2 - \frac{2M}{r_0} \cdot x^3 + \frac{\lambda_{\text{DM}}}{r_0} \cdot \ln \left( \frac{r_0}{\lambda_{\text{DM}}} \cdot \frac{1}{x} \right) \cdot x^3 \tag{59a}$$

$$F_0 = 1 - \frac{2M}{r_0} + \frac{\lambda_{\text{DM}}}{r_0} \cdot \ln \left( \frac{r_0}{\lambda_{\text{DM}}} \right) \tag{59b}$$

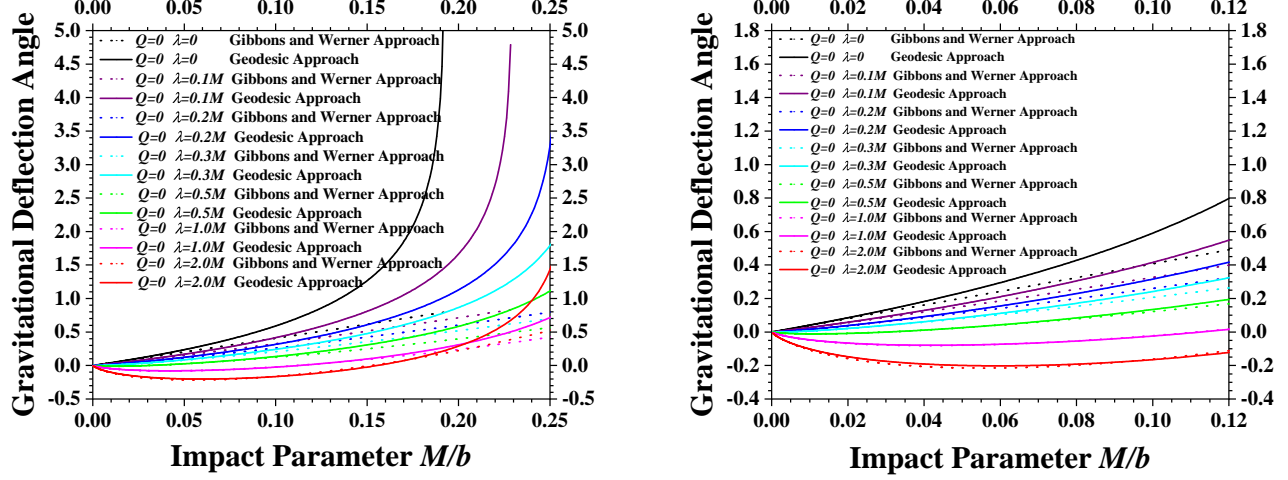


FIG. 3. The gravitational deflection angles for Schwarzschild black hole embedded in PFDM. This figure present the numerical results calculated from the Gibbons and Werner approach (using the Gauss-Bonnet theorem) in equation (49) and from the conventional geodesic approach (by solving the trajectories of null geodesics) in equation (58). Here, the dark matter parameter  $\lambda_{\text{DM}}$  is selected to be  $\lambda_{\text{DM}} = 0$ ,  $\lambda_{\text{DM}} = 0.1M$ ,  $\lambda_{\text{DM}} = 0.2M$ ,  $\lambda_{\text{DM}} = 0.3M$ ,  $\lambda_{\text{DM}} = 0.5M$ ,  $\lambda_{\text{DM}} = 1.0M$  and  $\lambda_{\text{DM}} = 2.0M$  to emphasize the effects of dark matter medium on the gravitational deflection angle. The right panel of this figure plots the amplified region where  $M/b$  is not very large.

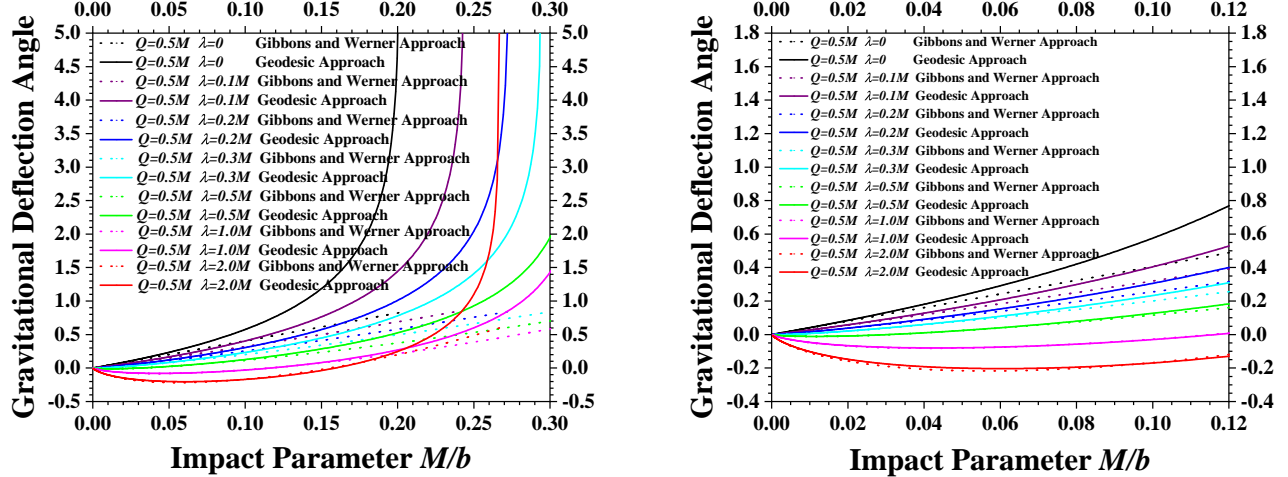


FIG. 4. The gravitational deflection angles for charged RN black hole embedded in PFDM. This figure present the numerical results on deflection angle calculated from the Gibbons and Werner approach in equation (56) and from the conventional geodesic approach in equation (58). In this figure, the black hole charge is chosen to be  $Q = 0.5M$  and the dark matter parameter is selected as  $\lambda_{\text{DM}} = 0$ ,  $\lambda_{\text{DM}} = 0.1M$ ,  $\lambda_{\text{DM}} = 0.2M$ ,  $\lambda = 0.3M$ ,  $\lambda_{\text{DM}} = 0.5M$ ,  $\lambda_{\text{DM}} = 1.0M$  and  $\lambda_{\text{DM}} = 2.0M$  to emphasize the effects of dark matter medium on gravitational deflection angle. The right panel of this figure shows the amplified region where  $M/b$  is not very large.

with  $r_0$  to be the minimal distance to central supermassive black hole in the photon orbit, and the variable  $x$  defined as  $x = r_0/r$ .

explicit expression for  $F_0$  and  $F(x)$  are

$$F(x) = x^2 - \frac{2M}{r_0} \cdot x^3 + \frac{Q^2}{r_0^2} \cdot x^4 + \frac{\lambda_{\text{DM}}}{r_0} \cdot \ln\left(\frac{r_0}{\lambda_{\text{DM}}} \cdot \frac{1}{x}\right) \cdot x^3 \quad (60a)$$

$$F_0 = 1 - \frac{2M}{r_0} + \frac{Q^2}{r_0^2} + \frac{\lambda_{\text{DM}}}{r_0} \cdot \ln\left(\frac{r_0}{\lambda_{\text{DM}}}\right) \quad (60b)$$

In the absence of dark matter halo, the function  $F(x) =$

For charged RN black hole embedded in PFDM, the

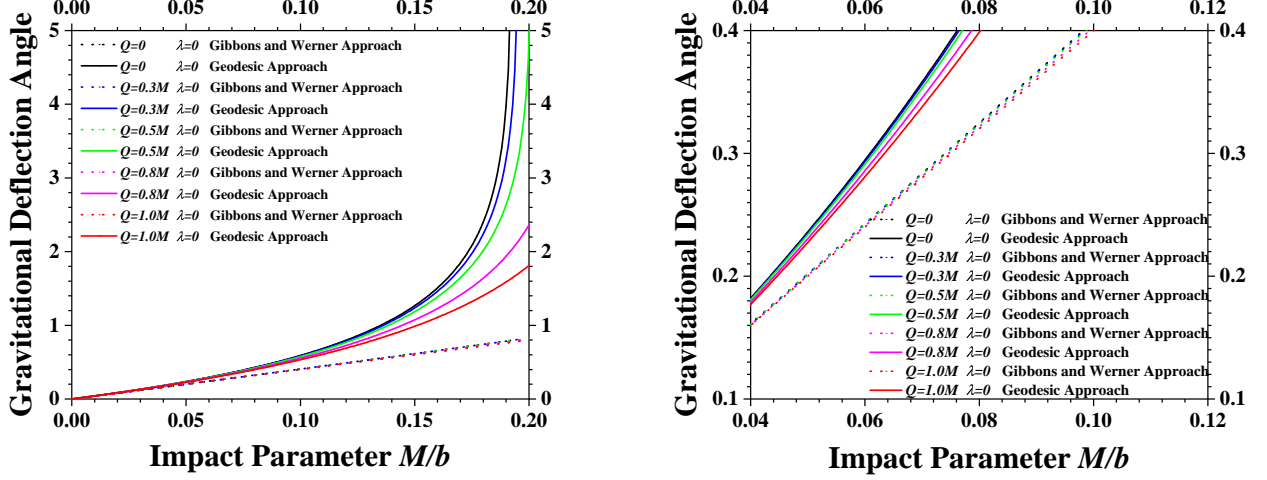


FIG. 5. The gravitational deflection angles for charged RN black hole embedded in PFDM. This figure present the numerical results calculated from the Gibbons and Werner approach in equation (56) and from the conventional geodesic approach in equation (58). In this figure, we select the dark matter parameter  $\lambda_{DM} = 0$  and the black hole charge to be  $Q = 0$ ,  $Q = 0.3M$ ,  $Q = 0.5M$ ,  $Q = 0.8M$  and  $Q = 1.0M$ , to show the effects on gravitational deflection angle coming from black hole charge  $Q$ . The right panel of this figure shows the amplified region such that the results obtained by Gibbons and Werner approach for various black hole charge can be effectively distinguished.

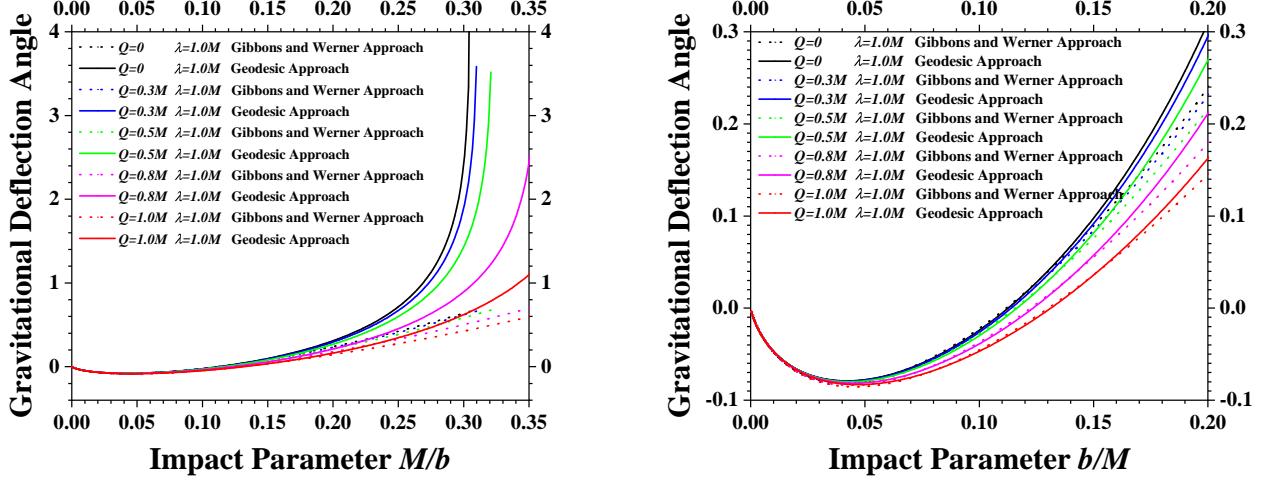


FIG. 6. The gravitational deflection angles for charged RN black hole embedded in PFDM. This figure present the numerical results calculated from the Gibbons and Werner approach in equation (56) and from the conventional geodesic approach in equation (58). In this figure, we select the dark matter parameter  $\lambda_{DM} = 1.0M$  and the black hole charge to be  $Q = 0$ ,  $Q = 0.3M$ ,  $Q = 0.5M$ ,  $Q = 0.8M$  and  $Q = 1.0M$ , to show the effects on gravitational deflection angle coming from black hole charge  $Q$ . The right panel of this figure shows the amplified region where  $M/b$  is not very large.

$P_n(x)$  becomes a polynomial function, which makes the gravitational deflection angle expressed by the hyperelliptic integral

$$F = \int_{x_1}^{x_2} \frac{dx}{\sqrt{a - P_n(x)}} \quad (61)$$

Here,  $a$  is a constant,  $P_n(z)$  is a polynomial function of  $x$  in  $n$ -th order. However, the existence of dark matter halo makes the function  $P(z)$  more complicated.

In the integration process, the closet distance  $r_0$  to central supermassive black hole in the photon orbit can be solved from the impact parameter  $b$  via equation

$$b^2 = \frac{L^2}{E^2} = \frac{r_0^2}{f(r_0)} \quad (62)$$

Furthermore, when the closet distance  $r_0$  approach to the radius of unstable photon sphere (namely  $r_0 \rightarrow r_{ph}$ ), the gravitational deflection angle of light become diver-

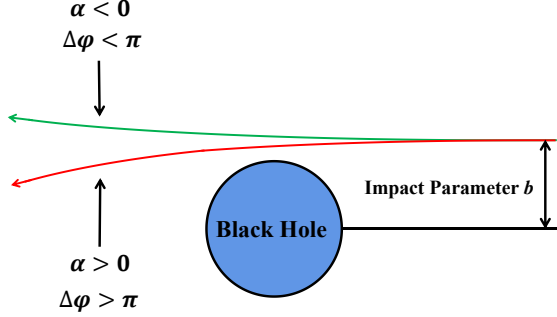


FIG. 7. The positive and negative deflection angles of light in the gravitational lensing.

gent [90], and the corresponding critical impact parameter is the shadow radius detected by observer at infinity ( $r_{sh} = b_{\text{critical}}$ ). The gravitational lensing in this case is extremely strong.

The numerical results on gravitational deflection angle of light for Schwarzschild and charged RN black hole embedded in PFDM are plotted in figure 3, figure 4, figure 5 and figure 6. The results from the Gibbons and Werner approach and the conventional geodesic approach are presented for comparisons. In the weak gravitational lensing cases where  $M/b$  is very small, the gravitational deflection angles calculated from the Gibbons and Werner approach and those from the conventional geodesic approach agree with each other. However, in the strong gravitational lensing cases where  $M/b$  is large, the gravitational deflection angles obtained from the above two approaches exhibit notable differences. There are two reasons lead to this discrepancy. Firstly, the gravitational deflection angle in equation (49) and equation (56) obtained from the Gibbons and Werner approach using the Gauss-Bonnet theorem are the second-order expansions of  $M/b$ . Higher-order contributions, which is non-negligible when  $M/b$  is larger, are not included. Secondly, in the strong gravitational lensing case, the photon orbits could be dramatically distorted, which are completely different with the slowly bended photon orbits present in figure 1. In these cases, the approximations  $\phi_{\text{observer}} \approx \pi + \alpha \approx \pi$  and  $r(\gamma) = r(\phi) \approx b/\sin \phi$  used in the integration of Gaussian curvature no longer valid. In the strong gravitational lensing, the results obtained by Gibbons and Werner approach using the Gauss-Bonnet theorem could underestimate the gravitational deflection angle.

Figure 3 and figure 4 shows the effects of PFDM parameter  $\lambda_{\text{DM}}$  on gravitational deflection angle, while figure 5 and figure 6 shows the effects from black hole charge. From these figures, we easily find that the black hole charge  $Q$  has negative contributions on gravitational deflection angle. For the same dark matter parameter  $\lambda_{\text{DM}}$ , charged RN black holes with bigger electric charge

results in smaller deflection angle. Furthermore, in the weak gravitational lensing where  $M/b$  is not large, the PFDM also has negative contributions on gravitational deflection angle, similar to the influences of black hole charge. For the same black hole charge, black holes with larger dark matter parameter eventually get smaller gravitational deflection angle (in the region  $M/b$  is not very large), which can be clearly indicated in the right panels of figure 3 and figure 4. This is mostly caused by the leading order factor  $-\frac{\lambda_{\text{DM}}}{b} - \frac{2\lambda_{\text{DM}}}{b} \cdot \ln\left(\frac{b}{2\lambda_{\text{DM}}}\right)$  in the expression of gravitational deflection angle presented in section IV.

From figure 3, figure 4 and figure 6, we can also discover an interesting phenomenon. When the PFDM parameter is sufficiently large ( $\lambda_{\text{DM}} > 0.5M$ ), the gravitational deflection angle of light could become negative when  $M/b$  is not very large. The positive and negative gravitational deflection angle could be interpreted in the following way. The positive deflection angle ( $\alpha > 0$ ) implies that the change of azimuthal angle in photon orbit is greater than  $180^\circ$  ( $\Delta\phi > \pi$ ) when light beams traveling near central black hole, and the gravitational field produced by central black hole as well as the PFDM medium eventually give “attractive effects” on light beams. On the other hand, the negative gravitational deflection angle ( $\alpha > 0$ ) implies that the change of azimuthal angle in photon orbit is less than  $180^\circ$  ( $\Delta\phi > \pi$ ) when light beams traveling near central black hole, and the gravitational field produced by central black hole as well as the PFDM medium eventually give “repulsive effects” on light beams. The positive and negative gravitational deflection angles of light are illustrated in figure 7.

## V. PHOTON SPHERE AND BLACK HOLE SHADOW

In this section, we present the numerical results on photon spheres and black hole shadow radius for Schwarzschild black hole and the charged RN black hole embedded in PFDM. They can be obtained by solving the local extreme points of effective potential, or using a geometric approach developed by Qiao *et al.* Figure 8 and figure 9 plot the photon sphere  $r_{ph}$  (in the left panel) and black hole shadow radius  $r_{sh} = b_{\text{critical}}$  (in the right panel) when black hole charge  $Q$  and dark matter parameter  $\lambda_{\text{DM}}$  are varying. From these figures, it is clearly shows that the PFDM can greatly change the photon spheres and black hole shadow radius for Schwarzschild black hole and the charged RN black hole.

From figure 8, for a fixed black hole charge  $Q$ , both the photon sphere radius and black hole shadow radius first diminish and then get enlarged, as dark matter parameters  $\lambda_{\text{DM}}$  varies from  $\lambda_{\text{DM}} = 0$  to  $\lambda_{\text{DM}} = 2M$ . The turning points are  $\lambda_{\text{DM}} \approx 0.5M$  for photon spheres and  $\lambda_{\text{DM}} \approx 0.75M$  for black hole shadows. When dark matter parameter  $\lambda_{\text{DM}}$  exceeds the tuning points, the photon sphere radius and black hole shadow radius begin to in-

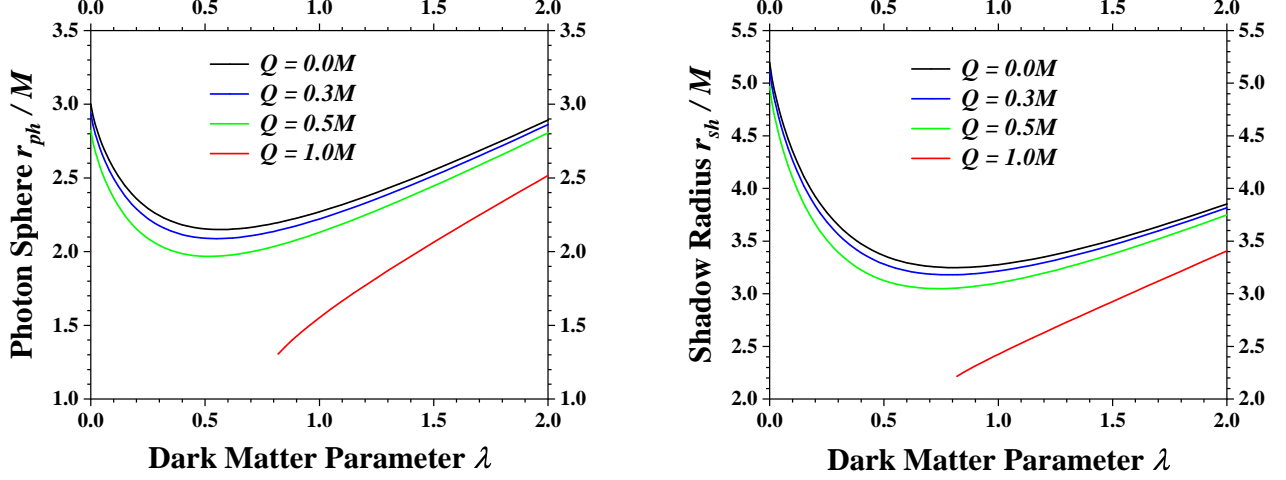


FIG. 8. The unstable photon spheres and black hole shadow radius for Schwarzschild black hole and charged RN black holes embedded in PFDM. In this figure, we choose the black hole charge to be  $Q = 0$ ,  $Q = 0.2M$ ,  $Q = 0.5M$ , and  $Q = 1.0M$  to show the photon sphere radius and shadow radius as dark matter parameter  $\lambda_{\text{DM}}$  varying. The left panel presents the unstable photon sphere radius  $r_{ph}$  and the right panel shows black hole shadow radius  $r_{sh} = b_{\text{critical}}$  for infinity observer. The case  $Q = 0$  represents the Schwarzschild black hole embedded in PFDM, and the case  $Q = 1.0M$  represent the extreme charged RN black hole embedded in PFDM.

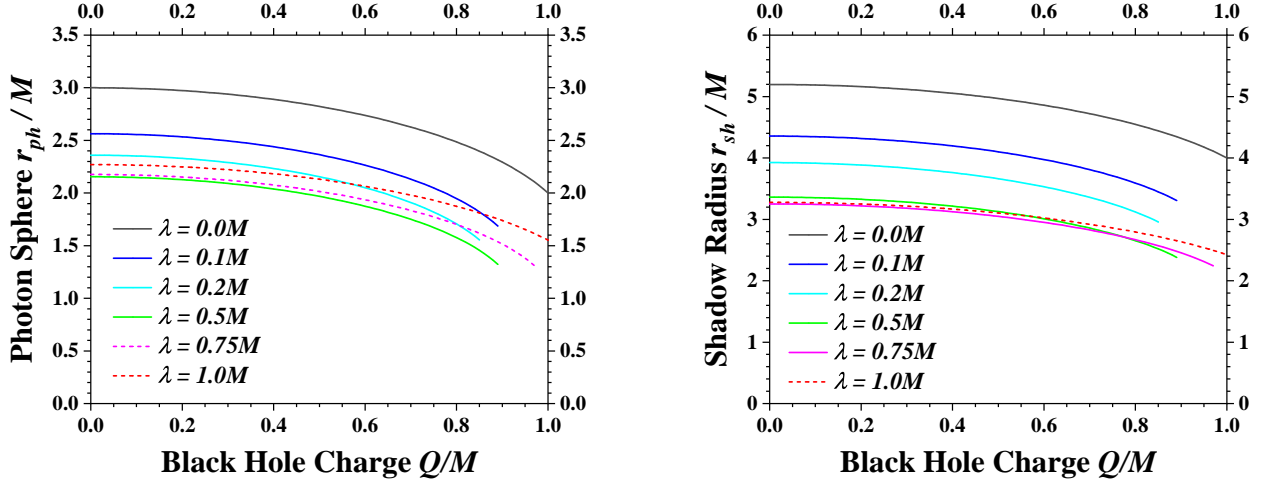


FIG. 9. The unstable photon spheres and black hole shadow radius for charged RN black hole embedded in PFDM. In this figure, we choose the dark matter parameter to be  $\lambda_{\text{DM}} = 0$ ,  $\lambda_{\text{DM}} = 0.1M$ ,  $\lambda_{\text{DM}} = 0.2M$ ,  $\lambda_{\text{DM}} = 0.5M$ ,  $\lambda_{\text{DM}} = 0.75M$  and  $\lambda_{\text{DM}} = 1.0M$  to show the photon sphere radius and shadow radius as black hole charge  $Q$  varying. The left panel presents the unstable photon sphere radius  $r_{ph}$ , and the right panel displays black hole shadow radius  $r_{sh} = b_{\text{critical}}$  for infinity observer. The case  $\lambda_{\text{DM}} = 0$  correspond to no dark matter medium, which recovers the standard RN black hole in general relativity.

crease.

In the figure 9, it can be concluded that the black hole charge has the effects to reduce the photon sphere and black hole shadow radius. For the same dark matter parameter  $\lambda_{\text{DM}}$ , RN black hole with bigger electric charge has smaller photon sphere and shadow radius. Another interesting phenomenon is that, in the extreme charged RN black hole case ( $M = Q$ ), the black hole shadow radius disappear for some dark matter param-

eter ( $0 < \lambda_{\text{DM}} < M$ ), making the green curve in figure 8 cut off. It is caused by the naked singularity in spacetime metric. In the extreme charged black hole case  $M = Q$ , the charged RN black hole embedded in PFDM in equation (6) could become horizonless and produce a naked singularity when dark matter parameter  $0 < \lambda_{\text{DM}} < M$ . Furthermore, in the naked singularity case (the extreme black hole  $M = Q$  with dark matter parameter  $0 < \lambda_{\text{DM}} < M$ ), the photon spheres could

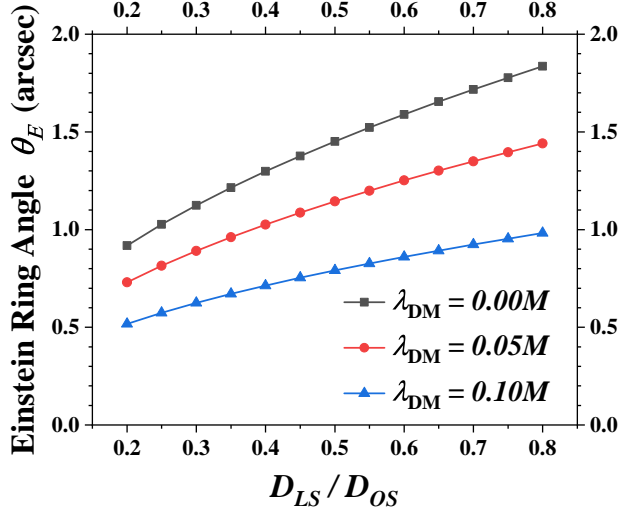


FIG. 10. The Einstein Ring Angle of Schwarzschild black hole embedded in PFDM. In this figure, the dark matter parameter is chosen to be  $\lambda_{\text{DM}} = 0$ ,  $\lambda_{\text{DM}} = 0.05M$  and  $\lambda_{\text{DM}} = 0.1M$ . The horizontal axis is the ratio of  $D_{\text{LS}}/D_{\text{OS}}$ , and the vertical axis is the Einstein ring angle  $\theta_E$  in unit of arc-second. Here, the mass of Schwarzschild black hole is  $M = 4.3 \times 10^6 M_\odot$ , and the distance between the observer and lensed plane is  $D_{\text{OL}} = D_{\text{LS}} - D_{\text{OS}} = 8.33$  kpc.

have no solution or multiple solutions. For some dark matter parameter (in range  $0 < \lambda_{\text{DM}} < M$ ), the photon spheres near black hole could disappear, for other dark matter parameter (also in range  $0 < \lambda_{\text{DM}} < M$ ), multiple photon spheres could emerge. However, we do not plot these multiple photon spheres in figure 8, since their connections with black hole shadows become subtle). This queer and unexpected behavior on photon spheres may be caused by an unknown mechanism or unknown black hole phase transition, and it deserves more intensive studies in the future [107].

## VI. WEAK GRAVITATIONAL LENS EQUATION AND EINSTEIN RING

In this section, we discuss the significant observable in gravitational lensing observations — the Einstein ring. In galaxies, the light beams from remote luminous light sources are greatly deflected and distorted due to the central supermassive black hole. Eventually, these light sources may exhibit multiple images after light beams converging from the central gravitational lens. The Einstein ring is one of the famous examples. It can be solved by weak gravitational lens equation.

In the weak gravitational lensing, we resort to the reduced gravitational lens equation presented in equation (40). Solving the lens equation with angle  $\beta = 0$ , the Einstein ring angle for Schwarzschild black hole embedded

in PFDM can be expressed as

$$\begin{aligned} \theta_E &= \frac{D_{\text{LS}}}{D_{\text{OS}}} \cdot \alpha \\ &\approx \frac{D_{\text{LS}}}{D_{\text{OS}}} \cdot \left\{ \frac{4M - \lambda_{\text{DM}}}{b} - \frac{2\lambda_{\text{DM}}}{b} \cdot \ln \left( \frac{b}{2\lambda_{\text{DM}}} \right) \right. \\ &\quad + \frac{(12M^2 + 10M\lambda_{\text{DM}} + \lambda_{\text{DM}}^2) \cdot \pi}{16b^2} + \frac{\pi\lambda_{\text{DM}}^2}{12b^2} \cdot \left[ \frac{\pi^2}{12} - \frac{1}{2} \right] \\ &\quad - \frac{(12M\lambda_{\text{DM}} + 5\lambda_{\text{DM}}^2) \cdot \pi}{16b^2} \cdot \ln \left( \frac{2b}{\lambda_{\text{DM}}} \right) \\ &\quad \left. + \frac{3\pi\lambda_{\text{DM}}^2}{16b^2} \cdot \left[ \ln \left( \frac{2b}{\lambda_{\text{DM}}} \right) \right]^2 \right\} \end{aligned} \quad (63)$$

Further, in the weak gravitational lensing case, the Einstein ring angle  $\theta_E$  is usually very small, and the impact parameter  $b$  in gravitational lensing satisfies

$$b \approx D_{\text{OL}} \sin \theta_E \approx D_{\text{OL}} \theta_E \quad (64)$$

The Einstein ring angle can be calculated by solving the equations (63) and (64).

Figure 10 gives the Einstein ring angle of Schwarzschild black hole embedded in PFDM, showing the dark matter effects on Einstein ring of supermassive black hole. In this figure, we choose the black hole mass to be  $M = 4.3 \times 10^6 M_\odot$ , and the distance between observer and the lensed plane is  $D_{\text{OL}} = 8.33$  kpc (which are the mass and distance of Sgr A\* in our galaxy). The dark matter parameter is chosen as  $\lambda_{\text{DM}} = 0$ ,  $\lambda_{\text{DM}} = 0.05M$  and  $\lambda_{\text{DM}} = 0.1M$  respectively. The numerical results on Einstein ring angle are plotted in figure 10 for different ratios  $D_{\text{LS}}/D_{\text{OS}}$ . From this table, it is clearly that, in the presence of dark matter halo, the Einstein ring angle becomes smaller than that of conventional Schwarzschild black hole. For the same dark matter parameter, the size of Einstein ring reduces when the ratio  $D_{\text{LS}}/D_{\text{OS}}$  is larger. In order to observe evident Einstein ring images, the distance  $D_{\text{LS}}$  should be as large as possible. Furthermore, when the dark matter parameter  $\lambda_{\text{DM}}$  is large, the Einstein ring angle  $\theta_E$  could have no solutions. Therefore, the Einstein ring angles for larger dark matter parameter  $\lambda_{\text{DM}}$  cases are not plotted in figure 10.

## VII. SUMMARY AND CONCLUSIONS

In this work, we study the weak gravitational lensing of black hole embedded in dark matter halo. We choose two typical black holes — the Schwarzschild black hole and the charged Reissner-Nordström (RN) black hole to carry out the investigation. To analyze the influences from dark matter, we assume the unknown dark matter halo is made up of perfect fluid with energy momentum tensor satisfies  $T_{\mu\nu} = (\rho + p)u_\mu u_\nu + pg_{\mu\nu}$ . The spacetime metric for Schwarzschild black hole and charged RN black hole embedded in perfect fluid dark matter (PFDM) are parameterized by black hole mass  $M$ , black hole charge  $Q$  and dark matter parameter  $\lambda_{\text{DM}}$ . These two simple black

hole examples (the Schwarzschild black hole and charged RN black hole embedded in PFDM) could reflect many universal properties of more complex black holes in dark matter medium, and they shall give us insights on the behaviors of supermassive black hole in the presence of dark matter halo.

In the presented work, the gravitational deflection angle of light, photon sphere, black hole shadow radius and Einstein angle radius are calculated and analyzed. Particularly, in the calculation of gravitational deflection angles, two approaches have been used. One is the Gibbons and Werner approach, in which the gravitational deflection angle is obtained using Gauss-Bonnet theorem in geometrical topology; the other one is the conventional geodesic approach, in which the gravitational deflection angle is obtained by solving the null geodesics. In the weak gravitational lensing cases where  $M/b$  is small, the numerical results obtained using two approaches agree with each other. However, in the strong gravitational cases where  $M/b$  is not small, there are non-negligible discrepancies between results obtained using two different approaches. In the strong gravitational lensing, some approximations used in the integration of Gaussian curvature are not satisfied when  $M/b$  is large. Therefore, the results obtained by Gibbons and Werner approach using the Gauss-Bonnet theorem could underestimate the gravitational deflection angle in the strong gravitational lensing cases.

The dark matter halo has a great effect on weak gravitational lensing of central supermassive black holes. For large dark matter parameter  $\lambda_{\text{DM}}$ , the Schwarzschild and charged RN black hole embedded in PFDM get smaller gravitational deflection angle in the weak gravitational lensing where  $M/b$  is not large. Particularly, when the PFDM parameter is sufficiently large ( $\lambda_{\text{DM}} > 0.5M$ ), the gravitational deflection angle of light could become negative. These effects are mostly caused by the leading order factor  $-\frac{\lambda_{\text{DM}}}{b} - \frac{2\lambda_{\text{DM}}}{b} \cdot \ln\left(\frac{b}{2\lambda_{\text{DM}}}\right)$  in the analytical expression of gravitational deflection angle. As dark matter parameters  $\lambda_{\text{DM}}$  increases, the photon sphere radius and black hole shadow radius for charged RN black hole embedded in PFDM first diminish and then increase after exceeding the tuning points (which are  $\lambda_{\text{DM}} \approx 0.5M$  for photon spheres and  $\lambda_{\text{DM}} \approx 0.75M$  for black hole shadow). In the weak gravitational lensing, the Ein-

stein ring angle of Schwarzschild black hole reduces when PFDM parameter  $\lambda_{\text{DM}}$  is increases, and the Einstein ring angle enlarges when ratio  $D_{\text{LS}}/D_{\text{OS}}$  becomes larger.

The black hole charge  $Q$  has negative contributions to the gravitational deflection angle, photon sphere and black hole shadow. For a given fixed dark matter parameter  $\lambda_{\text{DM}}$ , charged RN black holes with smaller electric charge  $Q$  contribute to smaller gravitational deflection angle, photon sphere and black hole shadow radius in the gravitational lensing. Furthermore, in the extreme charged RN black hole  $Q = M$  case, the spacetime metric becomes horizonless and produces a naked singularity when dark matter parameter  $0 < \lambda_{\text{DM}} < M$ , making the black hole shadow radius disappearing for these cases.

From the numerical results in the present study, the dark matter halo has significant effects on the weak gravitational lensing of supermassive black holes. The gravitational deflection angle of light, photon sphere, black hole shadow and Einstein ring angle can be great changed in the presence of dark matter. However, the PFDM is still a over-simplified model to describe the detailed dark matter distributions in real galaxies. In the future, it is helpful to use the more precise and widely used phenomenological dark matter distributions (eg, NFW, Burkert, Brownstein, Moore models [21, 22, 108–110]) to further study the dark matter influences on gravitational lensing of supermassive black holes in the center of galaxies.

## ACKNOWLEDGMENTS

The authors thanks Song-Lin Lyu for helpful discussions on numerical calculations. This work is supported by the Scientific Research Program of Chongqing Science and Technology Commission (the Chongqing “zhitongche” program for doctors, Grant No. CSTB2022BSXM-JCX0100), the Natural Science Foundation of Chongqing (Grant No. cstc2020jcyj-msxmX0879 and Grant No. CSTB2022NSCQ-MSX0932), the Scientific and Technological Research Program of Chongqing Municipal Education Commission (Grant No. KJQN202201126), and the Scientific Research Foundation of Chongqing University of Technology (Grants No. 2020ZDZ027).

---

[1] J. D. Bekenstein, Black holes and entropy, *Phys. Rev. D* **7**, 2333-2346 (1973).

[2] S. W. Hawking, Particle Creation by Black Holes, *Commun. Math. Phys.* **43**, 199-220 (1975); Erratum: *Commun. Math. Phys.* **46**, 206 (1976).

[3] W. G. Unruh, *Experimental Black-Hole Evaporation*, *Phys. Rev. Lett.* **46**, 1351-1353 (1981).

[4] S. Ryu and T. Takayanagi, Holographic derivation of entanglement entropy from AdS/CFT, *Phys. Rev. Lett.* **96**, 181602 (2006).

[5] B Abbott, R Abbott, T D Abbott, *et al.* (LIGO Scientific Collaboration and Virgo Collaboration) Observation of Gravitational Waves from a Binary Black Hole Merger, *Phys. Rev. Lett.* **116**, 061102 (2016). [arXiv:1602.03837\[gr-qc\]](https://arxiv.org/abs/1602.03837)

[6] K. Akiyama *et al.* (Event Horizon Telescope Collaboration), *First M87 Event Horizon Telescope Results. I. The Shadow of the Supermassive Black Hole*, *Astrophys. J.* **875**, L1 (2019). [arXiv:1906.11238\[astro-ph.GA\]](https://arxiv.org/abs/1906.11238)

[7] K. Akiyama *et al.* (The Event Horizon Telescope Collab-

oration), First sagittarius A\* Event Horizon Telescope results. I. The shadow of the supermassive black hole in the center of the Milky Way, *Astrophys. J. Lett.* **930**, L12 (2022).

[8] V. C. Rubin and W. K. Ford, Rotation of the Andromeda Nebula from a Spectroscopic Survey of Emission Regions, *Astrophys. J.* **159**, 379-403 (1970).

[9] E. Corbelli and P. Salucci, The extended rotation curve and the dark matter halo of M33, *Mon. Not. R. Astron. Soc.* **311**, 441-447 (2000). arXiv:9909252[astro-ph]

[10] D. Clowe, M. Bradac, A. H. Gonzalez, M. Markevitch, S. W. Randall, C. Jones and D. Zaritsky, A Direct Empirical Proof of the Existence of Dark Matter, *Astrophys. J.* **648**, L109-L113 (2006). arXiv:0608407[astro-ph]

[11] M. Davis, G. Efstathiou, C. S. Frenk and S. D. M. White, The evolution of large-scale structure in a universe dominated by cold dark matter, *Astrophys. J.* **292**, 371-394 (1985).

[12] E. Komatsu *et al.* (WMAP Collaboration), Seven-Year Wilkinson Microwave Anisotropy Probe (WMAP) Observations: Cosmological Interpretation, *Astrophys. J. Suppl.* **192**, 18 (2011). arXiv:1001.4538[astro-ph.CO]

[13] P. A. R. Ade *et al.* (Planck Collaboration), Planck 2013 results. XVI. Cosmological parameters, *Astron. Astrophys.* **571**, A16 (2014).

[14] G. Bertone, D. Hooper and J. Silk, Particle dark matter: Evidence, candidates and constraints, *Phys. Rept.* **405**, 279-390 (2005). arXiv:0404175[hep-ph]

[15] C. Boehm and P. Fayet, Scalar Dark Matter candidates, *Nucl.Phys.B* **683**, 219-263 (2004). arXiv:0305261[hep-ph]

[16] J. L. Feng, M. Kaplinghat, H. Tu, H. -B. Yu, Hidden Charged Dark Matter, *JCAP* **2009(07)**, 004 (2009). arXiv:0905.3039[hep-ph]

[17] P. W. Graham, I. G. Irastorza, S. K. Lamoreaux, A. Lindner and K. A. van Bibber, Experimental Searches for the Axion and Axion-like Particles, *Annual Review of Nuclear and Particle Science* **65**, 485-514 (2015). arXiv:1602.00039[hep-ex]

[18] M. Schumann, Direct Detection of WIMP Dark Matter: Concepts and Status, *J. Phys. G: Nucl. Part. Phys.* **46**, 103003 (2019). arXiv:1903.03026[astro-ph.CO]

[19] A. Boyarsky, M. Drewes, T. Lasserre, S. Mertens and O. Ruchayskiy, Sterile Neutrino Dark Matter, *Prog. Part. Nucl. Phys.* **104**, 1-45 (2019). 1807.07938[hep-ph]

[20] C. -K. Qiao, S. -T. Lin, H. -C. Chi and H. -T. Jia, Relativistic impulse approximation in the atomic ionization process induced by millicharged particles, *J. High Energ. Phys.* **2021**, 184 (2021). arXiv:2009.14320[hep-ph]

[21] J. F. Navarro, C. S. Frenk and S. D. M. White, The Structure of Cold Dark Matter Halos, *Astrophys. J.* **462**, 563-575 (1996). arXiv:9508025[astro-ph]

[22] J. F. Navarro, C. S. Frenk, and S. D. M. White, A Universal Density Profile from Hierarchical Clustering, *Astrophys. J.* **490**, 493-508 (1997). arXiv:9611107[astro-ph]

[23] A. Cooray and R. Sheth, Halo models of large scale structure, *Phys. Rept.* **372**, 1-129 (2002). arXiv:0206508[astro-ph]

[24] J. Rayimbaev, S. Shaymatov and M. Jamil, Dynamics of particles and epicyclic motions around Schwarzschild-de-Sitter black hole in perfect fluid dark matter, *Eur. Phys. J. C* **81**, 699 (2021). arXiv:2107.13436[gr-qc]

[25] A. Das, A. Saha and S. Gangopadhyay, Investigation of circular geodesics in a rotating charged black hole in the presence of perfect fluid dark matter, *Class. Quantum Grav.* **38**, 065015 (2021). arXiv:2009.03644[gr-qc]

[26] R. A. Konoplya, Shadow of a black hole surrounded by dark matter, *Physics Letters B* **795**, 1-6 (2019). arXiv:1905.00064[gr-qc]

[27] K. Jusufi, M. Jamil and Tao Zhu, Shadows of Sgr A\* black hole surrounded by superfluid dark matter halo, *Eur. Phys. J. C* **80**, 354 (2020). arXiv:2005.05299[gr-qc]

[28] K. Saurabh and Kimet Jusufi, Imprints of Dark Matter on Black Hole Shadows using Spherical Accretions, *Eur. Phys. J. C* **81**, 490 (2021). arXiv:2009.10599[gr-qc]

[29] A. Das, A. Saha and S. Gangopadhyay, Study of circular geodesics and shadow of rotating charged black hole surrounded by perfect fluid dark matter immersed in plasma, *Class. Quantum Grav.* **39**, 075005 (2022). arXiv:2110.11704[gr-qc]

[30] S. -J. Ma, T. -C. Ma, J. -B. Deng and X. -R. Hu, Black hole shadow, photon ring and lensing ring in the cold dark matter halo. arXiv:2206.12820[gr-qc]

[31] X. Hou, Z. Xu, M. Zhou and J. Wang, Black Hole Shadow of Sgr A\* in Dark Matter Halo, *JCAP* **2018(07)**, 015 (2018). arXiv:1804.08110[gr-qc]

[32] X. Hou, Z. Xu and J. Wang, Rotating black hole shadow in perfect fluid dark matter, *JCAP* **2018(12)**, 040 (2018). arXiv:1810.06381[gr-qc]

[33] S. Haroon, M. Jamil, K. Jusufi, K. Lin and R. B. Mann, Shadow and Deflection Angle of Rotating Black Holes in Perfect Fluid Dark Matter with a Cosmological Constant, *Phys. Rev. D* **99**, 044015 (2019). arXiv:1810.04103[gr-qc]

[34] S. U. Islam, R. Kumar and S. G. Ghosh, Gravitational lensing by black holes in the 4D Einstein Gauss-Bonnet gravity, *JCAP* **2020(09)**, 030 (2020). arXiv:2004.01038[gr-qc]

[35] R. C. Pantig and E. T. Rodulfo, *Weak deflection angle of a dirty black hole*, *Chinese J. Phys.* **66**, 691-702 (2020). arXiv:2003.00764[gr-qc]

[36] R. C. Pantig, P. K. Yu, E. T. Rodulfo and A. Övgün, Shadow and weak deflection angle of extended uncertainty principle black hole surrounded with dark matter, *Ann. Phys.* **436**, 168722 (2022). arXiv:2104.04304[gr-qc]

[37] R. C. Pantig and A. Övgün, Dark matter effect on the weak deflection angle by black holes at the center of Milky Way and M87 galaxies, *Eur. Phys. J. C* **82**, 391 (2022). arXiv:2201.03365[gr-qc]

[38] F. Atamurotov, U. Papnoi and K. Jusufi, Shadow and deflection angle of charged rotating black hole surrounded by perfect fluid dark matter, *Class. Quantum Grav.* **39**, 025014 (2022). arXiv:2104.14898[gr-qc]

[39] M. Heydari-Fard, S. G. Honarvar and M. Heydari-Fard, Thin accretion disk luminosity and its image around rotating black holes in perfect fluid dark matter, arXiv:2210.04173[gr-qc]

[40] Z. Xu, X. Hou, J. Wang and Y. Liao, Perfect Fluid Dark Matter Influence on Thermodynamics and Phase Transition for a Reissner-Nordstrom-Anti-de Sitter Black Hole, *Adv. High Energy Phys.* **2019**, 2434390 (2019). arXiv:1610.05454[gr-qc]

[41] Y. Cao, H. Feng, W. Hong and J. Tao, Joule-Thomson Expansion of RN-AdS Black Hole Immersed in Perfect Fluid Dark Matter, *Commun. Theor. Phys.* **73**, 095403 (2021). arXiv:2101.08199[gr-qc]

[42] K. Jusufi, Quasinormal modes of black holes surrounded by dark matter and their connection with the shadow radius, *Phys. Rev. D* **101**, 084055 (2020). arXiv:1912.13320[gr-qc]

[43] D. Liu, Y. Yang, A. Övgün, Z. -W. Long and Z. Xu, Quasinormal Modes and Greybody Bounds of Rotating Black Holes in a Dark Matter Halo, arXiv:2204.11563[gr-qc]

[44] D. Liu, Y. Yang, S. Wu, Y. Xing, Z. Xu, Z. -W. Long, Ringing of a black hole in a dark matter halo, *Phys. Rev. D* **104**, 104042 (2021). arXiv:2104.04332[gr-qc]

[45] J. Bamber, J. C. Aurrekoetxea, K. Clough and P. G. Ferreira, Black hole merger simulations in wave dark matter environments, arXiv:2210.09254[gr-qc]

[46] J. Wambsganss, Gravitational Lensing in Astronomy, *Living Rev. Relativ.* **1**, 12 (1998). arXiv:9812021[astro-ph]

[47] M. Bartelmann and P. Schneider, Weak gravitational lensing, *Phys. Rept.* **340**, 291-472 (2001).

[48] S. Mollerach and E. Roulet, *Gravitational Lensing and Microlensing* (World Scientific, Singapore, 2002).

[49] E. van Uitert, H. Hoekstra, T. Schrabback, D. G. Gilbank, M. D. Gladders and H. K. C. Yee, Constraints on the shapes of galaxy dark matter haloes from weak gravitational lensing, *Astron. Astrophys.* **545**, A71 (2012). arXiv:1206.4304[astro-ph.CO]

[50] F. Brimioule, S. Seitz, M. Lerchster, R. Bender and J. Snigula, Dark matter halo properties from galaxy-galaxy lensing, *Mon. Not. Roy. Astron. Soc.* **432**, 1046-1102 (2013). arXiv:1303.6287[astro-ph.CO]

[51] F. Rahaman, K. K. Nandi, A. Bhadra, M. Kalam, K. Chakraborty, Perfect fluid dark matter, *Phys. Lett. B* **694**, 10-15 (2010). arXiv:1009.3572[gr-qc]

[52] G. W. Gibbons and M. C. Werner, Applications of the Gauss-Bonnet theorem to gravitational lensing, *Class. Quantum Grav.* **25**, 235009 (2008). arXiv:0807.0854[gr-qc]

[53] C.-K. Qiao and M. Li, Geometric approach to circular photon orbits and black hole shadows, *Phys. Rev. D* **106**, L021501 (2022). arXiv:2204.07297[gr-qc]

[54] C.-K. Qiao, Curvatures, photon spheres, and black hole shadows *Phys. Rev. D* **106**, 084060 (2022). arXiv:2208.01771[gr-qc]

[55] P. V. P. Cunha, C. A. R. Herdeiro and J. P. A. Novo, *Null and timelike circular orbits from equivalent 2D metrics*, *Classical Quantum Gravity* **39**, 225007 (2022). arXiv:2207.14506[gr-qc]

[56] T. Matos, F. S. Guzmán and D. Núñez, Spherical Scalar Field Halo in Galaxies, *Phys. Rev. D* **62**, 061301 (2000). arXiv:0003398[astro-ph]

[57] Z. Xu, X. Hou, X. Gong and J. Wang, Black hole spacetime in dark matter halo, *JCAP* **2018(09)** 038 (2018). arXiv:1803.00767[gr-qc]

[58] M.-H. Li and K.-C. Yang, Galactic Dark Matter in the Phantom Field, *Phys. Rev. D* **86**, 123015 (2012). arXiv:1204.3178[astro-ph.CO]

[59] Y. Heydarzade and F. Darabi, Black Hole Solutions Surrounded by Perfect Fluid in Rastall Theory, *Physics Letters B* **771**, 365-373 (2017). arXiv:1702.07766[gr-qc]

[60] C. G. Böhmer, T. Harko and F. S. N. Lobo, Dark matter as a geometric effect in f(R) gravity, *Astropart. Phys.* **29**, 386-392 (2008). arXiv:0709.0046[gr-qc]

[61] M. C. Werner, Gravitational lensing in the Kerr-Randers optical geometry, *Gen. Relativ. Gravit.* **44**, 3047-3057 (2012). arXiv:1205.3876[gr-qc]

[62] A. Ishihara, Y. Suzuki, T. Ono, T. Kitamura, and H. Asada, Gravitational bending angle of light for finite distance and the Gauss-Bonnet theorem, *Phys. Rev. D* **94**, 084015 (2016). arXiv:1604.08308[gr-qc]

[63] A. Ishihara, Y. Suzuki, T. Ono and H. Asada, Finite-distance corrections to the gravitational bending angle of light in the strong deflection limit, *Phys. Rev. D* **95**, 044017 (2017). arXiv:1612.04044[gr-qc]

[64] A. Övgün, I. Sakalli and J. Saavedra, Shadow cast and deflection angle of Kerr-Newman-Kasuya spacetime, *JCAP* **2018(10)**, 041 (2018). arXiv:1807.00388[gr-qc]

[65] K. Jusufi, A. Övgün, J. Saavedra, Y. Vásquez and P. A. González, Deflection of light by rotating regular black holes using the Gauss-Bonnet theorem, *Phys. Rev. D* **97**, 124024 (2018). arXiv:1804.00643[gr-qc]

[66] G. Crisnejo, E. Gallo and A. Rogers, Finite distance corrections to the light deflection in a gravitational field with a plasma medium, *Phys. Rev. D* **99**, 124001 (2019). arXiv:1807.00724[gr-qc]

[67] G. Crisnejo and E. Gallo, Weak lensing in a plasma medium and gravitational deflection of massive particles using the Gauss-Bonnet theorem. A unified treatment, *Phys. Rev. D* **97**, 124016 (2018). arXiv:1804.05473[gr-qc]

[68] G. Crisnejo, E. Gallo and K. Jusufi, Higher order corrections to deflection angle of massive particles and light rays in plasma media for stationary spacetimes using the Gauss-Bonnet theorem, *Phys. Rev. D* **100**, 104045 (2019). arXiv:1910.02030[gr-qc]

[69] W. Javed, J. Abbas and A. Övgün, Deflection angle of photon from magnetized black hole and effects of non-linear electrodynamics, *Eur. Phys. J. C* (2019) **79**, 694 (2019). arXiv:1908.09632[physics.gen-ph]

[70] K. Takizawa, T. Ono, and H. Asada, Gravitational deflection angle of light: Definition by an observer and its application to an asymptotically nonflat spacetime, *Phys. Rev. D* **101**, 104032 (2020). arXiv:2001.03290[gr-qc]

[71] Z. Li, J. Jia, The finite-distance gravitational deflection of massive particles in stationary spacetime: a Jacobi metric approach, *Eur. Phys. J. C* **80**, 157 (2020). arXiv:1912.05194[gr-qc]

[72] Z. Li, G. Zhang and A. Övgün, Circular orbit of a particle and weak gravitational lensing, *Phys. Rev. D* **101**, 124058 (2020). arXiv:2006.13047[gr-qc]

[73] C. -K. Qiao and M. Zhou, The Gravitational Bending of Acoustic Schwarzschild Black Hole, arXiv:2109.05828[gr-qc]

[74] Z. Zhang, Geometrization of light bending and its application to SdSw spacetime, *Class. Quantum Grav.* **39**, 015003 (2022). arXiv:2112.04149[gr-qc]

[75] Qi-Ming Fu, Li Zhao and Yu-Xiao Liu, Weak deflection angle by electrically and magnetically charged black holes from nonlinear electrodynamics, *Phys. Rev. D* **104**, 024033 (2021). arXiv:2101.08409[gr-qc]

[76] Y. Kumaran and A. Övgün, Deriving Weak Deflection Angle by Black Holes or Wormholes using Gauss-Bonnet Theorem, *Turk J Phys* **45**, 247-267 (2021). arXiv:2111.02805[gr-qc]

[77] S. K. Jha and A. Rahaman, Gravitational lensing by the hairy Schwarzschild black hole, arXiv:2205.06052[gr-qc]

[78] N. Parbin, D. J. Gogoi, J. Bora and U. D. Goswami, Deflection angle and quasinormal modes of a de Sitter black hole in  $f(T,B)$  gravity, [arXiv:2211.02414\[gr-qc\]](https://arxiv.org/abs/2211.02414)

[79] Y. Huang and Z. Cao, Generalized Gibbons-Werner method for deflection angle, *Phys. Rev. D* **106**, 104043 (2022).

[80] Y. Huang and Z. Cao, Simplified formula of deflection angle with Gauss-Bonnet theorem and its application, [arXiv:2212.04254\[gr-qc\]](https://arxiv.org/abs/2212.04254)

[81] S. -S. Chern, W. -H. Chern and K. S. Lam, *Lectures on Differential Geometry* (World Scientific Publishing, Singapore, 1999).

[82] G. W. Gibbons and C. M. Warnick, Universal properties of the near-horizon optical geometry, *Phys. Rev. D* **79**, 064031 (2009). [arXiv:0809.1571\[gr-qc\]](https://arxiv.org/abs/0809.1571)

[83] S. M. Carroll, *Spacetime and Geometry: An Introduction to General Relativity* (Cambridge University Press, Cambridge, 2019).

[84] S. Weinberg, *Gravitation and Cosmology: Principles and Applications of the General Theory of Relativity* (Wiley, New York 1972).

[85] K. S. Virbhadra, D. Narasimha, and S. M. Chitre, Role of the scalar field in gravitational lensing, *Astron. Astrophys.* **337**, 1-8 (1998). [arXiv:9801174\[astro-ph\]](https://arxiv.org/abs/9801174)

[86] K. S. Virbhadra and G. F. R. Ellis, Schwarzschild black hole lensing, *Phys. Rev. D* **62**, 084003 (2000). [arXiv:9904193\[astro-ph\]](https://arxiv.org/abs/9904193)

[87] K.S. Virbhadra and G.F.R. Ellis, Gravitational lensing by naked singularities, *Phys.Rev.D* **65**, 103004 (2002).

[88] E. F. Eiroa, G. E. Romero and D. F. Torres, Reissner-Nordström black hole lensing, *Phys. Rev. D* **66**, 024010 (2002). [arXiv:0203049\[gr-qc\]](https://arxiv.org/abs/0203049)

[89] S. V. Iyer and A. O. Petters, Light's Bending Angle due to Black Holes: From the Photon Sphere to Infinity, *Gen. Rel. Grav.* **39**, 1563-1582 (2007). [arXiv:0611086\[gr-qc\]](https://arxiv.org/abs/0611086)

[90] V. Bozza, Comparison of approximate gravitational lens equations and a proposal for an improved new one, *Phys.Rev. D* **78**, 103005 (2008). [arXiv:0807.3872\[gr-qc\]](https://arxiv.org/abs/0807.3872)

[91] G. S. Bisnovatyi-Kogan and O. Y. Tsupko, Strong Gravitational Lensing by Schwarzschild Black Holes, *Astrophys.* **51**, 99-111 (2008). [arXiv:0803.2468\[astro-ph\]](https://arxiv.org/abs/0803.2468)

[92] K. S. Virbhadra, Relativistic images of Schwarzschild black hole lensing, *Phys. Rev. D* **79**, 083004 (2009). [arXiv:0810.2109\[gr-qc\]](https://arxiv.org/abs/0810.2109)

[93] N. Tsukamoto, Gravitational lensing by a photon sphere in a Reissner-Nordström naked singularity spacetime in strong deflection limits, [arXiv:2107.07146\[gr-qc\]](https://arxiv.org/abs/2107.07146)

[94] N. Tsukamoto, Gravitational lensing by using the 0th order of affine perturbation series of the deflection angle of a ray near a photon sphere, [arXiv:2211.04239\[gr-qc\]](https://arxiv.org/abs/2211.04239)

[95] J. B. Hartle, *Gravity: An Introduction to Einstein's General Relativity*, (Cambridge University Press, Cambridge, 2021).

[96] D. Pugliese, H. Quevedo, R. Ruffini, Circular motion of neutral test particles in Reissner-Nordström spacetime, *Phys. Rev. D* **83**, 024021 (2011). [arXiv:1012.5411 \[astro-ph.HE\]](https://arxiv.org/abs/1012.5411)

[97] Tim Johannsen, Photon Rings around Kerr and Kerr-like Black Holes, *Astrophys. J.* **777**, 170 (2013). [arXiv:0805.3146\[gr-qc\]](https://arxiv.org/abs/0805.3146)

[98] Q. Gan, P. Wang, H. Wu and H. Yang, Photon spheres and spherical accretion image of a hairy black hole, *Phys. Rev. D* **104**, 024003 (2021). [arXiv:2104.08703\[gr-qc\]](https://arxiv.org/abs/2104.08703)

[99] V. Perlick and O. Y. Tsupko, Calculating black hole shadows: Review of analytical studies, *Phys. Rept.* **947**, 1-39 (2022). [arXiv:2105.07101\[gr-qc\]](https://arxiv.org/abs/2105.07101)

[100] M. Wang, S. Chen and J. Jing, Chaotic shadows of black holes: a short review, *Commun. Theor. Phys.* **74**, 097401 (2022). [arXiv:2205.05855\[gr-qc\]](https://arxiv.org/abs/2205.05855)

[101] S. Frittelli and E. T. Newman, An Exact Universal Gravitational Lensing Equation, *Phys. Rev. D* **59**, 124001 (1999). [arXiv:9810017\[gr-qc\]](https://arxiv.org/abs/9810017)

[102] M. P. Dabrowski and F. E. Schunck, Boson stars as gravitational lenses, *Astrophys. J.* **535**, 316-324 (2000). [arXiv:9807039\[astro-ph\]](https://arxiv.org/abs/9807039)

[103] V. Bozza, S. Capozziello, G. Iovane and G. Scarpetta, Strong field limit of black hole gravitational lensing, *Gen. Rel. Grav.* **33**, 1535-1548 (2001). [arXiv:0102068\[gr-qc\]](https://arxiv.org/abs/0102068)

[104] V. Perlick, On the Exact gravitational lens equation in spherically symmetric and static space-times, *Phys. Rev. D* **69**, 064017 (2004). [arXiv:0307072\[gr-qc\]](https://arxiv.org/abs/0307072)

[105] V. Bozza and M. Sereno, The Weakly perturbed Schwarzschild lens in the strong deflection limit, *Phys. Rev. D* **73**, 103004 (2006). [arXiv:0603049\[gr-qc\]](https://arxiv.org/abs/0603049)

[106] M. Do Carmo, *Differential Geometry of Curves and Surfaces*, Prentice-Hall (1976).

[107] Actually, when the charge RN black hole approach to the extreme black hole case (namely  $Q \sim M$ ), the naked singularities and multiple photon spheres already have appeared when dark matter parameter  $0 < \lambda_{DM} < M$ . We only pick the extreme black hole case to plot in figure 8.

[108] A. Burkert, The Structure of Dark Matter Halos in Dwarf Galaxies, *Astrophys. J.* **447**, L25-L28 (1995). [arXiv:9504041\[astro-ph\]](https://arxiv.org/abs/9504041)

[109] B. Moore, F. Governato, T. Quinn, J. Stadel and G. Lake, Resolving the structure of cold dark matter halos, *Astrophys. J.* **499**, L5-L8 (1998). [arXiv:9709051\[astro-ph\]](https://arxiv.org/abs/9709051)

[110] J. R. Brownstein and J. W. Moffat, Galaxy Rotation Curves without Nonbaryonic Dark Matter, *Astrophys. J.* **636**, 721-741 (2006). [arXiv:0506370\[astro-ph\]](https://arxiv.org/abs/0506370)